

Are luminous radio-loud active galactic nuclei triggered by galaxy interactions?

C. Ramos Almeida^{1*}, P. S. Bessiere¹, C. N. Tadhunter¹, P. G. Pérez-González^{2,3}, G. Barro², K. J. Inskip⁴, R. Morganti^{5,6}, J. Holt⁷, & D. Dicken⁸

¹*Department of Physics and Astronomy, University of Sheffield, Sheffield, S3 7RH, UK*

²*Departamento de Astrofísica, Facultad de CC. Físicas, Universidad Complutense de Madrid, E-28040 Madrid, Spain*

³*Associate Astronomer at Steward Observatory, The University of Arizona*

⁴*Max-Planck-Institut für Astronomie, Königstuhl 17, D-69117 Heidelberg, Germany*

⁵*Netherlands Institute for Radio Astronomy, Postbus 2, 7990 AA Dwingeloo, the Netherlands*

⁶*Kapteyn Astronomical Institute, University of Groningen, Postbus 800, 9700 AV Groningen, the Netherlands*

⁷*Leiden Observatory, Leiden University, PO Box 9513, 2300 RA Leiden, the Netherlands*

⁸*Department of Physics and Astronomy, Rochester Institute of Technology, 84 Lomb Memorial Drive, Rochester NY 14623, USA*

ABSTRACT

We present the results of a comparison between the optical morphologies of a complete sample of 46 southern 2Jy radio galaxies at intermediate redshifts ($0.05 < z < 0.7$) and those of two control samples of quiescent early-type galaxies: 55 ellipticals at redshifts $z \leq 0.01$ from the Observations of Bright Ellipticals at Yale (OBEY) survey, and 107 early-type galaxies at redshifts $0.2 < z < 0.7$ in the Extended Groth Strip (EGS). Based on these comparisons, we discuss the role of galaxy interactions in the triggering of powerful radio galaxies (PRGs). We find that a significant fraction of quiescent ellipticals at low and intermediate redshifts show evidence for disturbed morphologies at relatively high surface brightness levels, which are likely the result of past or on-going galaxy interactions. However, the morphological features detected in the galaxy hosts of the PRGs (e.g. tidal tails, shells, bridges, etc.) are up to 2 magnitudes brighter than those present in their quiescent counterparts. Indeed, if we consider the same surface brightness limits, the fraction of disturbed morphologies is considerably smaller in the quiescent population (53% at $z < 0.2$ and 48% at $0.2 \leq z < 0.7$) than in the PRGs (93% at $z < 0.2$ and 95% at $0.2 \leq z < 0.7$ considering strong-line radio galaxies only). This supports a scenario in which PRGs represent a fleeting active phase of a subset of the elliptical galaxies that have recently undergone mergers/interactions. However, we demonstrate that only a small proportion ($\lesssim 20\%$) of disturbed early-type galaxies are capable of hosting powerful radio sources.

Key words: galaxies: active – galaxies: nuclei – galaxies: interactions – galaxies: evolution – galaxies: elliptical.

1 INTRODUCTION

Simulations of hierarchical galaxy evolution predict that the periods of black hole (BH) growth and nuclear activity are intimately tied to the growth of the host galaxy, and that the triggering of the main phase of this nuclear activity in gas-rich mergers will always be accompanied by a major galaxy-wide starburst (Kauffmann & Haehnelt 2000; Di Matteo et al. 2005; Springel et al. 2005; Hopkins et al. 2008a,b; Somerville et al. 2008). However, the order of events and the timescales involved in both the triggering of the merger-induced starburst and the nuclear ac-

tivity remain uncertain (see e.g. Canalizo & Stockton 2000; Wild et al. 2010; Tadhunter et al. 2011).

Based on cosmological simulations, Hopkins et al. (2008b) suggested a bimodality in the BH triggering mechanisms: luminous quasar-like activity is associated with the formation of classical bulges and ellipticals via galaxy mergers, whereas the less luminous Seyfert-like activity is associated with the formation of pseudobulges and bulgeless galaxies via secular processes. Under the assumption that major, gas-rich mergers trigger quasar activity, Hopkins et al. (2008b) reproduce the observed quasar luminosity function from $z=0$ to $z=6$. They also compare with a secular model in which the nuclear activity is driven by bars or instabilities and show that, although these processes probably dominate

* E-mail: C.Ramos@sheffield.ac.uk

at luminosities typical of Seyfert galaxies, they contribute very little to the $z \gtrsim 1$ quasar luminosity density.

From an observational point of view, a bimodality in formation mechanisms (and hence in AGN triggering) is supported by the fact that, whereas classical bulges and elliptical galaxies follow a close correlation between velocity dispersion and BH mass (Kormendy & Richstone 1995; Magorrian et al. 1998; Gebhardt et al. 2000; Ferrarese & Merritt 2000; Greene & Ho 2006), bulgeless galaxies and those with pseudobulges show no clear evidence for such a correlation (Kormendy et al. 2011).

Galaxy interactions are one of the most efficient mechanism to transport the cold gas required to trigger and feed AGN to the center of galaxies (Kauffmann & Haehnelt 2000; Cox et al. 2006, 2008; Croton et al. 2006; Di Matteo et al. 2007) and many observational studies of powerful AGN (i.e. quasar-like) have revealed a high incidence of interaction signatures in their host galaxies (Heckman et al. 1986; Hutchings 1987; Smith & Heckman 1989; Canalizo & Stockton 2001; Canalizo et al. 2007; Bennert et al. 2008, Ramos Almeida et al. 2011). However, all these studies lack comparisons with appropriate samples of quiescent (i.e. non-active) galaxies to confirm that the percentage of interacting systems in powerful AGN is larger than in the quiescent population. Indeed, based on high spatial resolution Hubble Space Telescope (HST) images of a sample of nearby radio galaxies and quasars, Dunlop et al. (2003) found evidences that their hosts are indistinguishable from quiescent ellipticals of similar mass. Moreover, for moderately luminous AGN (i.e. Seyfert galaxies, $L_{bol} \sim 10^{42} - 10^{45} \text{ erg s}^{-1}$) several studies find that the incidence of disturbed morphologies is not significantly enhanced over the general population (e.g. Malkan et al. 1998; Grogin et al. 2005; Georgakakis et al. 2009; Gabor et al. 2009; Cisternas et al. 2011), although some others find the opposite result (e.g. Keel et al. 1996; Kuo et al. 2008; Koss et al. 2010; Ellison et al. 2011).

In our previous work (Ramos Almeida et al. 2011; hereafter RA11) we studied the optical morphologies of a complete sample of 46 southern 2Jy radio galaxies at intermediate redshifts ($0.05 < z < 0.7$) and found that the overall majority of the sample (up to 85%) show peculiarities in their optical morphologies at relatively high levels of surface brightness. Our study indicates that galaxy interactions are likely to play a key role in the triggering of AGN/jet activity, especially in the case of strong-line radio galaxies (SLRGs)¹, of which 94% appear disturbed. On the other hand, of the weak-line radio galaxies (WLRGs)² in the 2Jy sample, only 27% show clear evidence for tidal features. These results are consistent with the most accepted explanation for the differences between the properties of SLRGs and WLRGs, in which SLRGs are powered by cold gas accretion, while WLRGs are fuelled by accretion of hot gas from their X-ray coronae (Allen et al. 2006;

Best et al. 2006; Hardcastle et al. 2007; Balmaverde et al. 2008; Buttiglione et al. 2010).

The high percentage of disturbed morphologies in the 2Jy sample of radio galaxies contrasts with the results found for lower luminosity AGN in, for example, the recent extensive study by Cisternas et al. (2011; hereafter C11). However, the RA11 and C11 studies can be reconciled by considering the differences in the depth of the observations and sample selection. First, the images employed in C11 were obtained with the Advanced Camera for Surveys (ACS) on the HST and are not as deep as our Gemini Multi-Object Spectrograph South (GMOS-S)/Gemini observations: the limiting surface brightness level of those HST images is 23.3 mag arcsec⁻² in the ACS F814W filter, whereas in RA11 we detected features as faint as 26.3 mag arcsec⁻² in the same band (using colour transformations for elliptical galaxies from Fukugita et al. 1995). Thus, the imaging observations used in C11, with a surface brightness limit 3 magnitudes brighter than ours, are not sensitive enough to reveal faint diffuse tidal features in their AGN and control samples, even if present. Second, the AGN in C11 were selected at X-ray wavelengths and the galaxy hosts are mostly disks with luminosities more typical of luminous Seyfert galaxies (median $L_{bol} \sim 10^{44.8} \text{ erg s}^{-1}$). In contrast, the AGN in RA11 were selected according to their radio emission and the majority have quasar-like luminosities that are typically an order of magnitude higher than those of the C11 sample (median value of $L_{bol} \sim 10^{45.7} \text{ erg s}^{-1}$ for the SLRGs in the 2Jy sample³) and they are almost exclusively hosted by elliptical galaxies. Thus, the differences between the findings of RA11 and C11 can be explained by the luminosity-dependent bimodality in the BH triggering mechanisms suggested by Hopkins et al. (2008b) and Kormendy et al. (2011), as well as by the differences in depth between the observations employed.

If galaxy interactions are the main triggering mechanism for radio-loud AGN activity in our sample, then it is expected that the signs of morphological disturbance will be stronger and more common in the radio source host galaxies than in the general population of quiescent ellipticals. Studies of nearby red galaxies (e.g. van Dokkum 2005) have shown that the majority of quiescent luminous ellipticals were assembled through gas-poor mergers, which explains their old stellar populations and high central densities. However, triggering and feeding a powerful radio source (and occasionally star formation; see Tadhunter et al. 2011) is likely to require a larger amount of cold gas to be accreted into the central regions of the galaxy. The morphological signatures of gas-rich interactions (such as tidal tails, shells, bridges, etc.) are brighter than those produced in gas-poor interactions (Naab et al. 2006; Bell et al. 2006; McIntosh et al. 2008). Thus, the surface brightness of the various morphological features can be used as an indicator of the type of interaction. In addition, the features resulting from gas-rich interactions are expected to be visible over time-scales between 0.5 and 1.5 Gyr (Le Fèvre et al. 2000; Patton et al.

¹ SLRGs comprise narrow-line radio galaxies (NLRGs), broad-line radio galaxies (BLRGs) and quasars, i.e. they are radio galaxies with strong and high equivalent width emission lines.

² WLRGs have optical spectra dominated by the stellar continua of the host galaxies and small emission line equivalent widths ($EW_{[OIII]} < 10 \text{ \AA}$; Tadhunter et al. 1998).

³ L_{bol} was derived from the [O III] luminosities of the individual galaxies listed in Dicken et al. (2009) by applying the bolometric correction factor of 3500 reported in Heckman et al. (2004) for low-redshift quasars.

2002; Conselice et al. 2003; Kawata et al. 2006), whereas those formed in gas-poor interactions are visible for only ~ 150 Myr (Bell et al. 2006).

This is the second in a series of papers based on the analysis of the optical morphologies of PRGs. In the first paper (RA11), we presented deep Gemini images for the 2Jy sample and compared the results found for the PRGs with various samples of quiescent ellipticals and/or red galaxies from the literature (Malin & Carter 1983; van Dokkum 2005; Tal et al. 2009). However, only the observations reported in the study of Malin & Carter (1983), which is based on photographic plates, have similar surface brightness depth to our PRG sample ($\mu_V \lesssim 25.5 \text{ mag arcsec}^{-2}$). After comparing with the latter study we concluded that the percentage of morphological disturbance of the PRGs (up to 85%) greatly exceeds that found for quiescent elliptical galaxies when the same surface brightness depth is considered ($\sim 10\%$). However, in order to make a more quantitative comparison, it is necessary to develop control samples of elliptical galaxies at similar redshifts and masses, probing the same scales and depths, and using CCD imaging data. In this paper we present the results from such a comparison. In Section 2 we describe the control sample selection and observations. In Section 3 we present the observational results. The comparison between the morphologies of PRGs and quiescent elliptical galaxies is discussed in Section 4, and the main conclusions from this work are summarized in Section 5. Throughout this paper we assume a cosmology with $H_0 = 70 \text{ km s}^{-1} \text{ Mpc}^{-1}$, $\Omega_m = 0.27$, and $\Omega_\Lambda = 0.73$.

2 SAMPLE SELECTION AND OBSERVATIONS

The objects studied in RA11 comprise all powerful radio galaxies (PRGs) and quasars from the Tadhunter et al. (1993) sample of 2Jy radio galaxies with $S_{2.7GHz} \geq 2.0$ Jy, steep radio spectra $\alpha_{2.7}^{4.8} > 0.5$ ($F_\nu \propto \nu^{-\alpha}$), declinations $\delta < +10^\circ$ and redshifts $0.05 < z < 0.7$ (see Table 1 in RA11). It is itself a subset of the Wall & Peacock (1985) complete sample of 2Jy radio sources. The $z > 0.05$ limit ensures that the radio galaxies are genuinely powerful sources, while the $z < 0.7$ limit ensures that sources are sufficiently nearby for detailed morphological studies.

In terms of the optical classification, the sample comprises 24% WLRGs and 76% SLRGs (Tadhunter et al. 1998). Considering the radio morphologies, Fanaroff-Riley II (FR II) sources constitute the majority of the sample (72%), 13% are Fanaroff-Riley I (FR I), and the remaining 15% are compact, steep-spectrum (CSS) or Gigahertz-peaked spectrum (GPS) sources (see Table 1 in RA11).

Moderately luminous AGN (e.g. those studied in C11) have a relatively high surface density and can be easily selected in deep field surveys, together with appropriate control samples of quiescent galaxies. On the contrary, quasars and radio galaxies are much rarer and cannot be studied using narrow, deep field surveys. In consequence, it is more challenging to develop control samples for such objects.

Since radio galaxies are almost invariably associated with elliptical hosts (see e.g. Heckman et al. 1986 and Dunlop et al. 2003), we searched in the literature for samples of elliptical galaxies with similar masses and redshifts as our 2Jy PRGs. In addition, similar angular resolutions and

depths are required to probe the same spatial scales and surface brightness levels. Our sample of 46 PRGs was imaged with the Gemini Multi-Object Spectrograph South (GMOS-S) on the 8.1-m Gemini South telescope at Cerro Pachón under good seeing conditions (median seeing of $0.8''$, ranging from $0.4''$ to $1.15''$). The GMOS-S detector (Hook et al. 2004) comprises three adjacent CCDs, giving a field-of-view (FOV) of $5.5 \times 5.5 \text{ arcmin}^2$, with a pixel size of $0.146''$. The morphological features reported in RA11 have a median surface brightness of $\mu_V = 23.6 \text{ mag arcsec}^{-2}$ and $\Delta\mu_V \sim [21, 26] \text{ mag arcsec}^{-2}$. See RA11 for a more detailed description of the GMOS-S observations. Thus, after considering all these factors, we finally selected control samples of elliptical galaxies in two redshift ranges which best match the 2Jy sample host galaxies: the Observations of Bright Ellipticals at Yale (OBEY) survey and the Extended Groth Strip (EGS) sample.

2.1 The OBEY survey

The OBEY survey (Tal et al. 2009) is a volume-limited and statistically complete sample of 55 luminous elliptical galaxies selected from the Nearby Galaxies Catalog (Tully 1988; see Table 1). It consists of all elliptical galaxies in the Tully (1988) catalog with declinations between -85 and $+10$, at distances from 16 to 40 Mpc, and $M_B < -20.4 \text{ mag}$, once corrected to the cosmology considered here. The sample comprises galaxies from a wide range of different environments: 36% are field galaxies, 33% are in groups, and 18% are in clusters, including members of the Virgo, Fornax, Centaurus, and Antlia clusters. These galaxy environments were determined from the literature by Tal et al. (2009) and no classification is reported in that study for the remaining 13%. This wide variety of environments in the OBEY survey matches those typical of FR II radio galaxies, which are found in field/groups as well as in moderately rich clusters (Prestage & Peacock 1988; Smith & Heckman 1990; Zirbel 1997) and constitute the majority of our PRG sample (72%).

Thus, we have a sample of 55 giant elliptical galaxies at redshifts $z \leq 0.01$ and with absolute magnitudes $M_B = [-22.5, -20.4] \text{ mag}$. If we assume no evolution for massive elliptical galaxies since $z=0.2$ (Cimatti et al. 2006; Faber et al. 2007), we can compare the OBEY sample with the PRGs in the 2Jy sample at $z < 0.2$. In Figure 1 we show a comparison between the absolute magnitudes of the 24 PRGs with $z < 0.2$ and the 55 quiescent ellipticals from Tal et al. (2009). The M_B values for the PRGs have been calculated from the Galactic extinction-, cosmological dimming-, and k-corrected r'-band magnitudes reported in RA11. Colours of elliptical galaxies from Fukugita et al. (1995) have been used to convert the magnitudes to the B-band, resulting in absolute magnitudes within the interval $M_B = [-22.1, -20.3] \text{ mag}$. From the comparison between the two M_B distributions shown in Figure 1, the significance level of the Kolmogorov-Smirnov (KS) statistic is 0.04 (i.e. there is only a 4% chance that the two distributions are drawn from the same parent population). The low value of the KS probability is due to the larger number of $M_B > -21 \text{ mag}$ ellipticals in the OBEY sample compared to the PRGs. However, both distributions span the same range in absolute magnitude and we prefer to keep the complete sample of 55 quiescent elliptical galaxies rather than reducing the number of fainter

GALAXY	R.A.	Dec	z	M_B	(B-V)	Obs. date	Tc	Morphology	Group
NGC 0584	01:31:20.7	-06:52:05	0.0060	-20.98	0.92	2006-08-22	0.076	2S,B	1
NGC 0596	01:32:52.1	-07:01:55	0.0062	-20.52	0.90	2006-08-23	0.110	S,F	2
NGC 0720	01:53:00.5	-13:44:19	0.0058	-20.68	0.96	2006-08-24	0.079	2F	2
NGC 1199	03:03:38.4	-15:36:49	0.0085	-20.39	0.97	2006-01-25	0.067	...	5
NGC 1209	03:06:03.0	-15:36:41	0.0086	-20.66	0.95	2006-01-26	0.116	T,3F,[D]	2
NGC 1399	03:38:29.1	-35:27:03	0.0047	-20.64	0.98	2008-09-30	0.064	...	5
NGC 1395	03:38:29.8	-23:01:40	0.0057	-20.59	0.94	2006-01-27	0.094	3S	2
NGC 1407	03:40:11.9	-18:34:49	0.0059	-21.32	0.93	2006-01-28	0.083	...	5
NGC 2865	09:23:30.2	-23:09:41	0.0087	-21.00	0.78	2006-03-28	0.193	3S,2T,[D]	2
NGC 2974	09:42:33.3	-03:41:57	0.0064	-20.93	0.95	2006-02-05	0.110	S,[D]	2
NGC 2986	09:44:16.0	-21:16:41	0.0076	-21.00	0.99	2006-01-30	0.045	[B]	5
NGC 3078	09:58:24.6	-26:55:37	0.0086	-20.93	0.97	2006-01-31	0.103	...	5
NGC 3258	10:28:53.6	-35:36:20	0.0093	-20.62	0.92	2006-02-01	0.123	[2N]	5
NGC 3268	10:30:00.6	-35:19:32	0.0093	-20.58	0.96	2006-02-03	0.087	S	2
NGC 3557B	11:09:32.1	-37:20:59	0.0096	-20.43	0.86	2006-02-04	0.182	2I	2
NGC 3557	11:09:57.6	-37:32:21	0.0103	-22.48	0.87	2006-01-31	0.111	F,[S]	2
NGC 3585	11:13:17.1	-26:45:18	0.0047	-21.23	0.91	2006-03-29	0.048	2S	2
NGC 3640	11:21:06.8	+03:14:05	0.0041	-21.08	0.92	2006-04-01	0.142	S,4F	2
NGC 3706	11:29:44.4	-36:23:29	0.0099	-21.44	0.93	2006-01-26	0.120	2S	2
NGC 3904	11:49:13.2	-29:16:36	0.0052	-20.41	0.94	2006-01-28	0.108	S	2
NGC 3923	11:51:01.8	-28:48:22	0.0058	-21.53	0.95	2006-01-29	0.100	4S	2
NGC 3962	11:54:40.1	-13:58:30	0.0060	-21.03	0.95	2006-03-30	0.059	S	2
NGC 4105	12:06:40.8	-29:45:37	0.0064	-20.66	0.87	2006-02-02	0.109	2F,T	1
NGC 4261	12:19:23.2	+05:49:31	0.0074	-21.71	0.98	2006-04-03	0.053	T,F	2
NGC 4365	12:24:28.2	+07:19:03	0.0041	-20.82	0.97	2006-03-29	0.070	F	2
IC 3370	12:27:37.3	-39:20:16	0.0097	-21.53	0.89	2006-04-02	0.192	F,S,D	2
NGC 4472	12:29:46.7	+08:00:02	0.0033	-22.12	0.97	2008-06-09	0.000	...	5
NGC 4636	12:42:49.9	+02:41:16	0.0031	-20.98	0.93	2006-03-28	0.066	F	2
NGC 4645	12:44:10.0	-41:45:00	0.0087	-21.18	0.95	2009-04-18	0.000	...	5
NGC 4697	12:48:35.9	-05:48:03	0.0041	-21.97	0.92	2006-04-04	0.091	...	5
NGC 4696	12:48:49.3	-41:18:40	0.0098	-22.35	0.94	2008-06-08	0.075	S,D	2
NGC 4767	12:53:52.9	-39:42:52	0.0099	-21.43	0.93	2008-06-10	0.000	2S,[D]	2
NGC 5011	13:12:51.8	-43:05:46	0.0105	-21.40	0.89	2006-04-05	0.077	...	5
NGC 5018	13:13:01.0	-19:31:05	0.0093	-21.76	0.85	2008-06-03	0.184	3T,3S,[D]	2
NGC 5044	13:15:24.0	-16:23:08	0.0092	-21.31	0.98	2008-06-06	0.041	...	5
NGC 5061	13:18:05.1	-26:50:14	0.0069	-21.49	0.85	2006-04-01	0.104	T,S	2
NGC 5077	13:19:31.7	-12:39:25	0.0093	-20.82	0.98	2006-03-30	0.061	[S],[D]	5
NGC 5576	14:21:03.7	+03:16:16	0.0049	-20.70	0.88	2008-06-06	0.122	3T,S	2
NGC 5638	14:29:40.4	+03:14:00	0.0055	-21.42	0.94	2008-06-07	0.036	T,S	2
NGC 5812	15:00:55.7	-07:27:26	0.0065	-20.88	0.94	2008-06-08	0.080	T	2
NGC 5813	15:01:11.2	+01:42:07	0.0065	-21.07	0.95	2008-06-09	0.054	...	5
NGC 5846	15:06:29.3	+01:36:20	0.0057	-21.46	0.98	2008-06-07	0.068	3S,2N	2,3
NGC 5898	15:18:13.5	-24:05:53	0.0070	-20.79	0.92	2006-04-05	0.114	3T,D,2N	2,3
NGC 5903	15:18:36.5	-24:04:07	0.0085	-21.18	0.89	2006-04-05	0.075	...	5
IC 4797	18:56:29.7	-54:18:21	0.0089	-21.05	0.92	2006-08-23	0.226	T,I,[D]	2
IC 4889	19:45:15.1	-54:20:39	0.0085	-20.85	0.88	2006-08-18	0.158	F	2
NGC 6861	20:07:19.5	-48:22:13	0.0094	-21.10	0.95	2006-08-19	0.123	D	4
NGC 6868	20:09:54.1	-48:22:46	0.0095	-21.36	0.97	2006-08-20	0.096	...	5
NGC 6958	20:48:42.6	-37:59:51	0.0090	-20.83	0.86	2006-08-22	0.122	3S,[D]	2
NGC 7029	21:11:52.0	-49:17:01	0.0094	-20.41	0.86	2006-08-22	0.085	...	5
NGC 7144	21:52:42.4	-48:15:14	0.0064	-20.66	0.91	2006-08-17	0.100	...	5
NGC 7196	22:05:54.8	-50:07:10	0.0097	-20.62	0.91	2006-08-19	0.171	S,[D]	2
NGC 7192	22:06:50.1	-64:18:58	0.0099	-20.85	0.92	2006-08-20	0.096	S	2
IC 1459	22:57:10.6	-36:27:44	0.0060	-20.88	0.96	2006-08-18	0.137	4S	2
NGC 7507	23:12:07.6	-28:32:23	0.0052	-20.51	0.94	2006-08-21	0.084	S	2

Table 1. Full classification of the OBEY survey ordered by R.A. Columns 2, 3, and 4 list R.A., declination and spectroscopic redshift as reported in the NASA/IPAC Extragalactic Database (NED). Columns 5, 6, and 7 correspond to the B-band absolute magnitudes from Tully (1988) and corrected to $H_0 = 70 \text{ km s}^{-1} \text{ Mpc}^{-1}$, the Vega (B-V) colors within effective radius from Michard (2005) and de Vaucouleurs et al. (1991), and the dates of observation. Column 8 lists the tidal parameter reported in Tal et al. (2009). Columns 9 and 10 list our morphological classification (T: Tail; F: Fan; B: Bridge; S: Shell; D: Dust feature; 2N: Double Nucleus; 3N: Triple Nucleus; A: Amorphous Halo; I: Irregular feature. Brackets indicate uncertain identification of a feature), and division in groups: 1) galaxy pair or group in tidal interaction; 2) galaxies showing T,F,S,D,A,I; 3) multiple nuclei (inside a 10 kpc); 4) galaxies with dust as the only detected feature, 5) isolated galaxies with no sign of interaction. Features with uncertain identification have not been considered in the statistics discussed in this study.

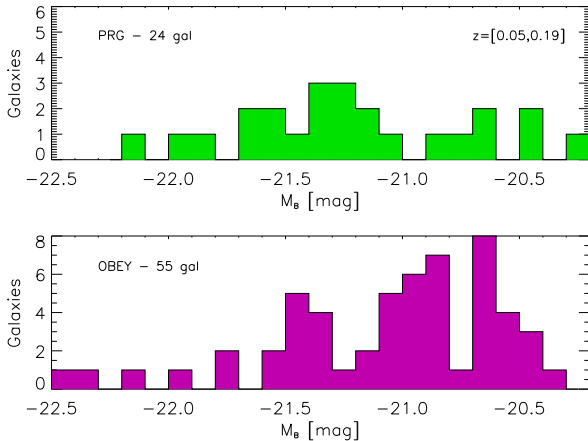


Figure 1. Comparison between the B-band absolute magnitudes of the PRGs in the 2Jy sample at $z < 0.2$ (top panel) and those of the Tal et al. (2009) sample of quiescent ellipticals at $z \leq 0.01$ (bottom panel).

objects. In addition, as we discuss in Section 3.1.3, we do not find any significant correlation between luminosity and the level of morphological disturbance.

The 55 galaxies in the OBEY survey were imaged with Y4KCam, which is a 4Kx4K CCD camera optimized for wide-field broad-band imaging mounted on the 1 m SMARTS telescope at the Cerro Tololo Inter-American Observatory (CTIO) between 2006 and 2009. The final images are a combination of several pointings of 300 s in the V-band, resulting in very deep frames with exposure times between 4200 and 7200 s. Tal et al. (2009) reported a detection threshold of $\mu_V \sim 27.7$ mag (in this work we have measured a surface brightness of $\mu_V = 28.2$ mag arcsec $^{-2}$ for the faintest feature detected, as shown in Section 3.1.4).

The data were binned in order to improve the signal-to-noise of the images, which have a final pixel size of 1.156'' and a typical value of the seeing of $\sim 1.7''$. More details on the sample selection and observations can be found in Tal et al. (2009) and are summarized in Table 1. The images are then deeper than the GMOS-S images of the PRGs in the 2Jy sample, for which the faintest detected feature has a $\mu_V = 26.2$ mag arcsec $^{-2}$, and both the pixel size and the average seeing are larger than those of the 2Jy radio galaxies (0.146''/pixel and FWHM $\sim 0.8''$ respectively for the GMOS-S images). However, considering that the galaxies in the OBEY sample are at a median distance of 36 Mpc (spatial scale of ~ 170 pc arcsec $^{-1}$) and the PRGs (those at $z < 0.2$) at 423 Mpc (spatial scale of ~ 1700 pc arcsec $^{-1}$) the effective resolution will be better in the case of the OBEY survey images. Thus, considering that the latter images are deeper and the resolution better, we will likely detect fainter and smaller features than for the PRGs. Even in the case of large-scale diffuse structures, the fact that the OBEY images are two magnitudes deeper than those of the 2Jy sample will allow us to detect them. Summarising, by using the same classification technique employed for the PRGs, we will be able to detect the same morphological signatures, if present, in the OBEY survey. Any possible bias will lead to a relative enhancement of the number of detected features in this sample relative to the PRG sample studied in RA11.

Since no observations of photometric standard stars were taken during the OBEY survey observations, we self-calibrated the images using aperture photometry measurements of the sample of elliptical galaxies from Prugniel & Heraudeau (1998), as in Tal et al. (2009).

2.2 The Extended Groth Strip sample

In order to develop a control sample for the PRGs in the 2Jy sample at redshifts $0.2 \leq z < 0.7$ we have used the *Rainbow Cosmological Surveys database*⁴, which is a compilation of photometric and spectroscopic data, jointly with value-added products such as photometric redshifts, stellar masses, star formation rates, and synthetic rest-frame magnitudes, for several deep cosmological fields (Pérez-González et al. 2008; Barro et al. 2009, 2011). Specifically, we have selected our control sample in the EGS ($\alpha = 14^h 17^m$, $\delta = +52^\circ 30'$), which enlarges the HST Groth-Westphal strip (Groth et al. 1994) up to $2^\circ \times 15'$ and has the advantage of being a low extinction area. We chose the EGS because it is a survey that covers sufficient area, and consequently enough galaxies, to extract statistically meaningful results, and because of the vast amount of public data available, including photometric redshifts, absolute magnitudes, colours, and deep imaging in the optical (Davis et al. 2007). Indeed, here we use broadband images in the R_c filter obtained with the Subaru Telescope, which are similar in pixel size and depth to the GMOS-S images of the PRGs employed in RA11.

Thus, we selected all the galaxies in the EGS with the same redshift and absolute magnitude ranges as the PRGs at $z \geq 0.2$ in RA11 ($0.2 \leq z < 0.7$ and $-22.2 \leq M_B \leq -20.6$ mag respectively). The limiting values of this M_B range were defined by considering NLRGs and WLRGs in RA11, since the quasars and BLRGs are likely to be contaminated by a large contribution from AGN emission. From this first selection we discard the sources in the EGS detected in X-rays (i.e. possible AGN) and foreground stars. The stars were automatically identified based on a combination of several criteria including their morphology (stellarity index) and their optical/NIR colours (see Pérez-González et al. 2008 and Barro et al. 2011 for details on the star-galaxy separation criteria). In order to identify elliptical galaxies, we imposed a colour selection criterion: initially we selected all the sources with rest-frame colours ($M_u - M_g$) > 1.5 , typical of galaxies located in the red sequence in the colour-magnitude diagram (Blanton 2006).

We choose this initial colour selection rather than morphologically selecting elliptical galaxies from the outset in order to avoid possible biases. The goal of this paper is to compare the morphologies of quiescent ellipticals with those of PRGs; by morphologically selecting elliptical galaxies (either by eye or automatically) we could be discarding highly disturbed sources, leading to an underestimation of interacting systems in the control sample. After applying the colour selection, we made a first visual classification of the sources into three groups: elliptical galaxies (E), possible disks (PD), and disks (D). According to Bundy et al. (2010), the red sequence is populated not only by elliptical and S0 galaxies,

⁴ https://rainbowx.fis.ucm.es/Rainbow_Database

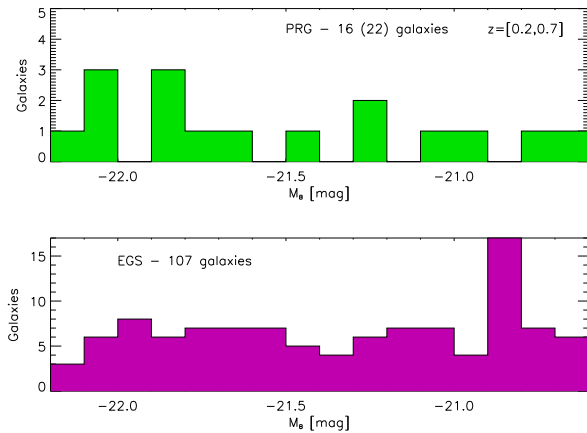


Figure 2. Comparison between the B-band absolute magnitudes of the PRGs in the 2Jy sample at $0.2 \leq z < 0.7$ (top panel) and those of the red galaxies in the EGS (bottom panel).

but also by early-type spirals. We then discarded all the galaxies that appeared as clear disks and kept the elliptical galaxies and possible disks in the sample. The latter might include disturbed ellipticals that look more disk-like, or S0/early-type spirals. After considering all these criteria, we have a control sample of 107 red early-type (ET) galaxies in the EGS (see Table 2).

In Figures 2 and 3 we show the comparison in absolute magnitude and redshift between the PRGs and the EGS control sample. Note that in Figure 2 we do not include the 6 BLRGs and quasars with $M_B < -22.2$ mag. The EGS redshifts are photometric with an average quality of $\Delta z/(1+z) = 0.03$. The absolute magnitudes were estimated by convolving the best fitting galaxy templates, used to calculate the photometric redshifts, with the appropriate filter transmission (see Pérez-González et al. 2008; Barro et al. 2009, 2011 for specific details). The significance level of the KS statistic from the comparison between the two M_B distributions shown in Figure 2 is 0.18, indicating that there is no significant difference between the two samples in terms of the distribution of absolute magnitude. The same is valid for the comparison between the redshift distributions (Figure 3), for which the value of the KS probability is 0.15.

The EGS was imaged with the Subaru Prime Focus Camera (Suprime-Cam; Miyazaki et al. 2002), which is a mosaic of ten 2048×4096 CCDs, located at the prime focus of Subaru Telescope. Details on the observations of the EGS can be found in (Zhao et al. 2009). It covers a 34×27 arcmin² FOV with a pixel scale of $0.202''$. The Suprime-Cam data consist of four Rc-band images of 1200 s exposure time that cover the entire field to a 5σ limiting AB magnitude of ~ 26.5 (Park et al. 2008). In this work we have measured a surface brightness of $\mu_V = 26.3$ mag arcsec⁻² for the faintest feature detected, as shown in Section 3.1.4. The seeing measured for the 4 images ranges from $0.60''$ to $0.72''$. Thus, the data are comparable in depth and resolution to the GMOS-S images employed in the study of the morphologies of the PRGs. In Figure 4 we present six examples of Suprime-Cam images of galaxies in the EGS, showing different levels of disturbance in their morphologies.

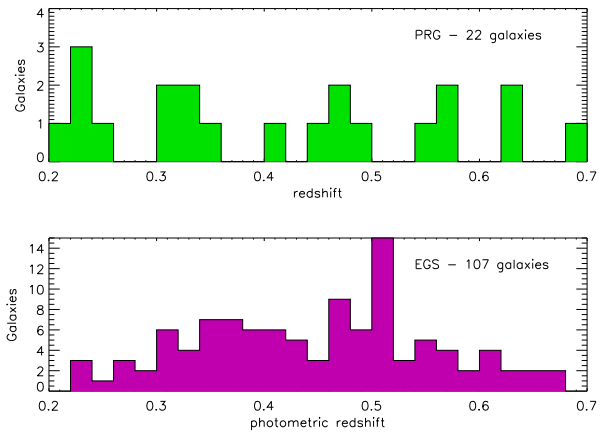


Figure 3. Comparison between the spectroscopic redshifts of the PRGs in the 2Jy sample at and the photometric redshifts of the red galaxies in the EGS (bottom panel).

3 RESULTS

3.1 Optical Morphologies

The main aim of this work is to perform a morphological classification of the galaxies in the OBEY and EGS samples in the same manner as for the PRGs in the 2Jy sample studied in RA11 and then to compare the results. This comparison will allow us to determine whether or not galaxy interactions are more common in powerful AGN than in quiescent galaxies and, consequently, to establish how important these interactions are in the triggering of nuclear activity.

3.1.1 Morphological Features

The morphological classification of the galaxies was done blind, with no information about any previous work on the sources, by CRA visually inspecting the 55 OBEY survey and the 107 EGS images. In addition, PB and CT also examined the EGS galaxy morphologies and there was agreement among the classifiers for the majority of the galaxies. Any possible conflicts were resolved by re-examining the images. The classification of the various features detected in the two control samples is based on that first used by Heckman et al. (1986) and is exactly the same as employed in RA11. Note that the classification of the PRGs was done using the fully-reduced GMOS-S original images, before any image enhancement technique were applied to them. The following morphological features are considered.

- A *tail* (T) corresponds to a narrow curvilinear feature with roughly radial orientation.
- A *fan* (F) is similar to a tail, but shorter and broader.
- A *bridge* (B) is a feature that links the radio galaxy with a companion.
- A *shell* (S) is a curving filamentary structure with a roughly tangential orientation to the main body of the galaxy.
- *Dust* (D) includes both nuclear dusty features and large scale dust lanes.
- *Amorphous haloes* (A) are irregular galaxy hosts or

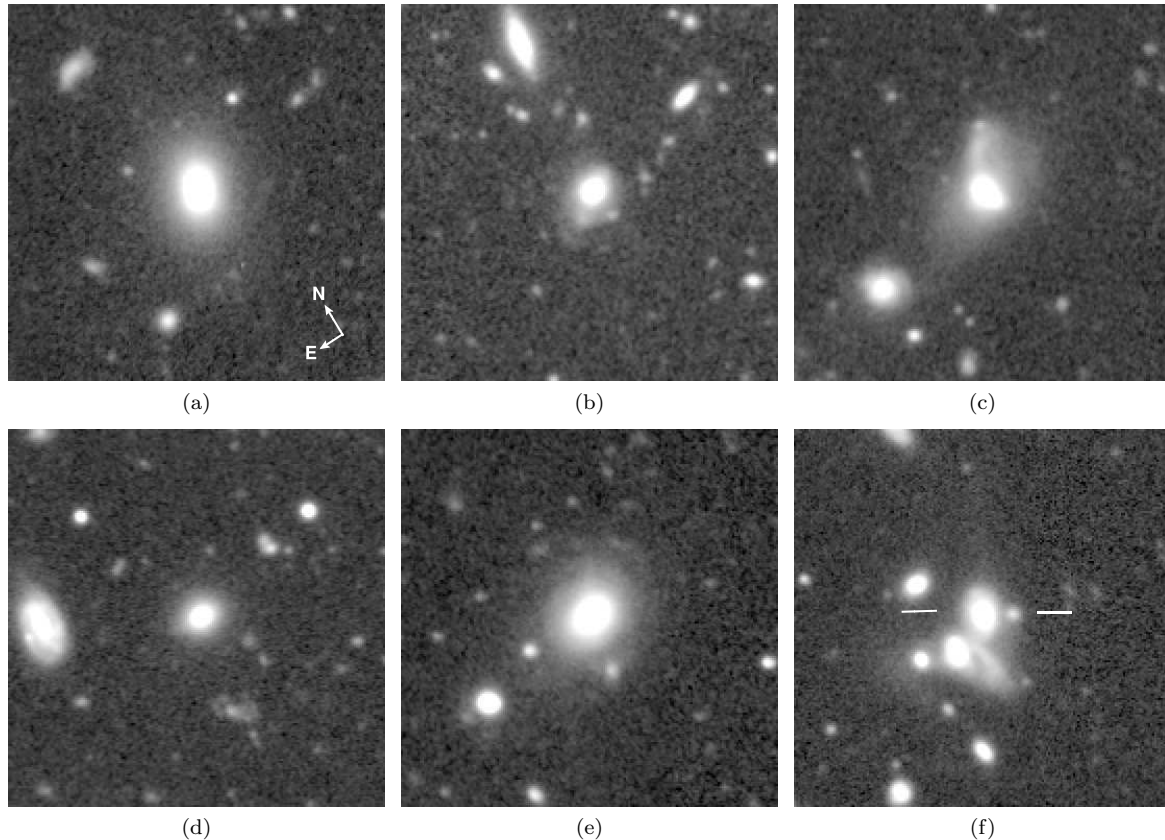


Figure 4. Examples of early-type galaxies in the EGS sample. The level of disturbance in their morphologies increases from left to right. Images size is $36''$ side. IDs and classification from Table 2 follow: (a) irac105193 - undisturbed; (b) irac145098 - A,T; (c) irac111427 - 2N,T,2I; (d) irac161724 - undisturbed; (e) irac204944 - T,S; (f) irac124509 - B,2T,F.

inner features that cannot be clearly distinguished from the main body of the galaxy (e.g. knotty haloes).

- By *irregular* (I) we refer to any feature, generally elongated, that cannot be classified as any of the previous.
- *Double nuclei* (2N) are those composed of two bright peaks inside 10 kpc, following the definition employed by Smith & Heckman (1989), based on statistical studies of cluster galaxies (Hoessel 1980)⁵ and N-body simulations of interacting binary galaxies (Borne 1984).

All of these features, with the possible exception of the dust, are very likely the result of galaxy interactions. Simulations have shown how spiral-spiral (S-S), elliptical-spiral (E-S) and elliptical-elliptical (E-E) interactions can produce all of the features that form the basis of our classification (Quinn 1984; Hernquist & Spergel 1992; Cattaneo et al. 2005; Lotz et al. 2008; Feldmann et al. 2008). For a more detailed description of how the different features described above are produced, according to simulations, see Section 5.1.1. in RA11. The classified features for both the OBEY survey and the EGS sample are listed in Tables 1 and 2 respectively. Features with uncertain identification (between brackets in Tables 1 and 2) have not been considered for the statistics. Examples of the EGS galaxy morphologies

are shown in Figure 4 and all the sample images can be individually viewed online in the Rainbow Database⁶. For the images of the OBEY survey we refer the reader to Tal et al. (2009).

The projected linear scales of the tidal features reported in Tables 1 and 2 range from less than 10 kpc in the case of galaxies with double nuclei, to ~ 80 -85 kpc in the case of long tidal tails such as that in NGC 1209 (OBEY survey) and bridges linking galaxies as in the case of irac128074 (EGS sample). For the PRGs in the 2Jy sample the longest feature that we measured was the spectacular bridge in PKS 0349-27, which links the radio galaxy with a distorted companion at ~ 83 kpc (RA11).

3.1.2 Quantitative versus visual analysis of tidal disturbance

In Section 3.1.1 we described how we performed the visual classification of the optical morphologies of the PRG, OBEY, and EGS samples. In the following, we compare the results of this visual classification of the galaxies in the OBEY survey with the quantitative analysis of the degree of tidal disturbance carried out by Tal et al. (2009) for the same galaxies. The latter authors fitted an elliptical galaxy model to the targets and, after masking the foreground

⁵ Hoessel (1980) claimed that typical cluster members are expected to experience a close encounter or merger within this radius every 10^9 years.

⁶ https://rainbowx.fis.ucm.es/Rainbow_navigator_public/

IRAC ID	R.A.	Dec	z_{phot}	M_B	($Mu-Mg$)	Type	Morphology	Group
004162	14:21:29.6	52:58:35	0.48	-20.65	1.75	E	...	5
006612	14:17:29.5	52:44:33	0.31	-21.56	1.71	E	B,F,[D],[T]	1,3
006613	14:17:29.3	52:44:29	0.30	-20.81	1.70	E	B	1
056690	14:15:14.4	52:12:52	0.50	-21.01	1.70	E	[A],[B]	5
060191	14:23:43.2	53:35:33	0.57	-21.82	1.72	E	F	2
060958	14:23:25.2	53:37:59	0.40	-20.84	1.84	PD	T,[A],[B]	1,2
061249	14:23:34.8	53:35:28	0.65	-21.95	1.68	PD	[T]	5
066105	14:23:25.2	53:26:14	0.51	-21.46	1.64	E	[A]	5
067417	14:23:01.4	53:28:33	0.39	-21.25	1.60	E	...	5
072533	14:22:26.9	53:25:19	0.33	-20.67	1.64	E	S	2
073519	14:22:21.1	53:24:32	0.49	-21.20	1.55	E	[A]	5
074777	14:22:24.5	53:21:09	0.42	-21.91	1.61	E	[S]	5
074924	14:22:24.5	53:20:53	0.41	-21.35	1.67	E	...	5
077695	14:22:18.2	53:16:39	0.35	-20.92	1.69	PD	T	2
079968	14:22:02.4	53:15:17	0.60	-21.62	1.82	E	F	2
082325	14:21:22.8	53:18:39	0.55	-22.05	1.82	E	[F]	5
083714	14:21:24.5	53:15:34	0.50	-22.01	1.52	E	F	2
088031	14:21:17.5	53:09:09	0.50	-21.04	1.68	E	F	2
090430	14:21:09.1	53:07:43	0.38	-21.83	1.75	E	A,F,[B]	2
092065	14:21:10.3	53:05:40	0.55	-21.44	1.80	E	B	1
092765	14:20:41.0	53:11:01	0.35	-21.60	1.77	PD	[A],[T]	5
093764	14:20:34.3	53:11:23	0.39	-21.50	1.52	E	[S]	5
094231	14:21:00.0	53:05:36	0.41	-21.98	1.81	E	2F,[T]	2
094966	14:21:21.1	53:00:27	0.46	-21.65	1.76	E	2T	2
095727	14:20:48.7	53:06:24	0.38	-21.59	1.76	E	F,S	2
099954	14:20:14.4	53:09:06	0.27	-20.83	1.71	E	[T]	5
102757	14:19:57.6	53:09:40	0.22	-20.81	1.71	E	2S	2
102982	14:20:56.6	52:57:14	0.60	-21.80	1.67	E	F	2
103198	14:20:43.2	52:59:46	0.38	-21.45	1.76	E	2N,F,S	2,3
104038	14:20:29.3	53:01:46	0.46	-20.72	1.75	E	B	1
104729	14:20:43.0	52:58:14	0.63	-21.76	1.61	PD	A	2
105193	14:20:07.0	53:05:07	0.23	-21.08	1.90	E	[S]	5
106324	14:19:48.0	53:07:49	0.26	-20.85	1.60	E	[T]	5
106984	14:20:47.0	52:54:57	0.45	-20.98	1.72	PD	A,[I]	2
111427	14:20:23.5	52:55:02	0.32	-20.81	1.66	E	2N,T,2I	1,3
112580	14:20:01.2	52:58:23	0.51	-21.62	1.70	E	[B]	5
113088	14:20:00.7	52:57:57	0.48	-21.22	1.76	E	[B]	5
113577	14:19:56.4	52:58:21	0.67	-22.05	1.56	PD	[A]	5
114966	14:20:25.1	52:50:53	0.61	-22.18	1.69	PD	2T,S	2
115327	14:19:37.2	53:00:20	0.35	-20.96	1.76	E	2F,[T]	2
115594	14:20:27.8	52:49:36	0.31	-20.81	1.78	E	2N,T	2,3
118942	14:20:21.8	52:47:15	0.37	-21.04	1.63	E	...	5
119696	14:20:18.2	52:47:12	0.50	-21.77	1.68	E	B,F	1,2
122098	14:19:26.6	52:55:17	0.22	-21.34	1.65	PD	...	5
124509	14:19:29.8	52:51:59	0.34	-20.75	1.84	PD	B,2T,F	1,2
125663	14:19:34.8	52:49:47	0.53	-21.53	1.59	E	[F]	5
126918	14:18:57.1	52:56:12	0.49	-21.22	1.77	E	F,[B]	1,2
127241	14:20:00.0	52:42:54	0.59	-21.75	1.67	PD	...	5
127457	14:18:47.0	52:57:40	0.50	-22.08	1.63	E	2N,A	2,3
128074	14:19:09.6	52:52:25	0.34	-20.73	1.65	E	B,[F]	1
128416	14:19:58.3	52:42:01	0.58	-21.51	1.68	PD	...	5
132682	14:18:39.8	52:53:49	0.33	-20.83	1.51	E	...	5
135859	14:18:49.0	52:48:38	0.40	-20.88	1.80	E	[I]	5

stars and background galaxies in the sky-subtracted and flat-fielded images, they divided the masked frames by the galaxy model. This process produces an image of the residuals that they translated into a number, the tidal parameter, defined as: $T = |(I_{x,y}/M_{x,y}) - 1|$, where $I_{x,y}$ and $M_{x,y}$ are the pixel values at (x,y) of the galaxy and model images, respectively. They finally applied a correction for the residual noise to the latter values, to derive the corrected tidal parameter

(T_c ; see Tal et al. 2009 for a more detailed description of the methodology).

Based on the values of T_c determined for the galaxies in the OBEY survey, Tal et al. (2009) divided them into three groups: 1) galaxies showing clear signs of morphological disturbance ($T_c > 0.09$; 53% of the sample), 2) galaxies with marginal disturbance ($0.07 < T_c < 0.09$; 20%), and 3) galaxies lacking interaction signatures ($T_c < 0.07$; 27%). In Figure 5 we represent these tidal parameters versus the B-

IRAC ID	R.A.	Dec	z_{phot}	M_B	($Mu-Mg$)	Type	Morphology	Group
138794	14:19:17.5	52:39:40	0.50	-21.23	1.70	E	[T]	5
139190	14:19:00.2	52:42:49	0.44	-20.66	1.66	E	...	5
140456	14:19:08.2	52:39:53	0.30	-21.13	1.78	PD	2T	2
140758	14:19:15.4	52:38:05	0.43	-21.31	1.68	E	S	2
141714	14:18:47.3	52:42:51	0.44	-20.65	1.76	PD	[B],[S]	5
143149	14:18:07.9	52:49:24	0.37	-21.81	1.77	E	T	2
143536	14:18:33.1	52:43:52	0.50	-21.20	1.81	PD	[T]	5
145098	14:18:10.6	52:46:50	0.32	-20.84	1.70	E	A,T	2
145434	14:18:53.3	52:37:43	0.48	-21.68	1.68	PD	4T	2
146298	14:18:35.0	52:40:34	0.59	-21.57	1.76	E	[A]	5
152722	14:17:41.3	52:44:45	0.49	-20.77	1.55	PD	[F]	5
156161	14:18:36.5	52:29:35	0.30	-20.71	1.79	E	T	2
157751	14:18:24.5	52:30:24	0.47	-21.22	1.81	E	...	5
157878	14:17:30.2	52:41:20	0.46	-20.85	1.70	E	F	2
159123	14:18:15.8	52:30:37	0.56	-22.03	1.70	PD	T	2
159936	14:17:28.3	52:39:26	0.41	-21.22	1.55	E	2N	3
160442	14:17:33.8	52:37:46	0.47	-21.90	1.61	E	B,A	1,2
160500	14:17:33.1	52:37:53	0.34	-20.81	1.78	PD	B,2T	1,2
161724	14:17:25.4	52:38:08	0.34	-20.71	1.95	PD	[F]	5
165265	14:17:11.0	52:37:29	0.67	-22.04	1.55	E	B,T	1,2
166730	14:17:53.5	52:27:22	0.36	-21.01	1.55	E	S,T	2
169386	14:16:58.6	52:35:49	0.47	-20.68	1.55	PD	...	5
172474	14:17:19.9	52:28:24	0.51	-20.90	1.82	E	T,B,F	1,2
173901	14:17:32.2	52:24:15	0.32	-21.39	1.76	E	...	5
175347	14:17:08.9	52:27:09	0.60	-21.92	1.60	E	S,[B]	2
175590	14:17:15.4	52:25:33	0.56	-21.68	1.71	E	[A]	5
177990	14:16:41.3	52:29:02	0.25	-21.05	1.75	PD	F,[2N]	2
178118	14:17:20.2	52:20:51	0.46	-21.74	1.75	E	...	5
178724	14:17:15.1	52:20:51	0.52	-21.81	1.67	E	A	2
178868	14:16:57.5	52:24:09	0.37	-22.14	1.69	PD	F	2
180420	14:16:54.0	52:21:50	0.54	-21.91	1.62	E	2N,2T,[B]	2,3
181402	14:16:38.2	52:23:08	0.38	-20.87	1.76	E	[I],[A]	5
181444	14:16:47.3	52:21:11	0.31	-21.63	1.71	E	2S,[I]	2
181736	14:16:27.4	52:24:39	0.46	-20.93	1.79	PD	...	5
181914	14:16:57.6	52:18:10	0.36	-20.72	1.66	PD	...	5
182762	14:16:52.8	52:17:28	0.43	-21.41	1.71	PD	[F]	5
183081	14:16:49.0	52:17:38	0.36	-21.86	1.71	E	F,[T]	2
183836	14:16:43.2	52:17:21	0.44	-21.02	1.76	E	[S]	5
184041	14:16:40.0	52:17:35	0.53	-22.13	1.75	E	F,S	2
184315	14:16:16.8	52:21:46	0.50	-21.61	1.64	PD	2N	3
186058	14:16:08.9	52:19:59	0.54	-21.77	1.80	PD	[A]	5
189727	14:16:15.1	52:11:21	0.64	-21.96	1.80	PD	...	5
190795	14:16:10.3	52:10:12	0.51	-21.19	1.70	PD	T,S	2
193464	14:15:36.5	52:11:41	0.42	-20.69	1.66	E	2N,F	2,3
193507	14:16:03.1	52:06:11	0.47	-21.91	1.71	E	2N,[B]	3
193737	14:15:54.5	52:07:30	0.50	-20.88	1.55	E	...	5
193974	14:15:31.4	52:11:46	0.40	-21.20	1.73	E	[S]	5
194092	14:15:29.0	52:12:00	0.51	-20.88	1.66	E	[T]	5
196827	14:15:41.3	52:03:43	0.37	-20.86	1.76	E	T	2
198295	14:14:58.6	52:09:25	0.54	-21.91	1.72	E	[S]	5
199503	14:14:56.2	52:07:26	0.50	-21.20	1.70	PD	T	2
202111	14:14:41.3	52:04:54	0.27	-21.16	1.70	E	[S]	5
204161	14:14:57.8	51:57:54	0.62	-21.78	1.88	E	A,[B]	2
204944	14:14:41.3	51:59:40	0.28	-21.55	1.66	PD	T,S	2

Table 2. Full classification of the EGS sample ordered by IRAC ID (Rainbow database identifier). Columns 2, 3, and 4 list R.A., declination and photometric redshift. Columns 5 and 6 correspond to the B-band absolute magnitudes and ($Mu-Mg$) rest-frame colors from the Rainbow database. Column 7 indicates whether a galaxy has been visually classified as an elliptical or as a possible disk. Columns 8 and 9 list the morphological classification and group as in Table 1. Features with uncertain identification (within brackets) have not been considered in the statistics discussed in this work.

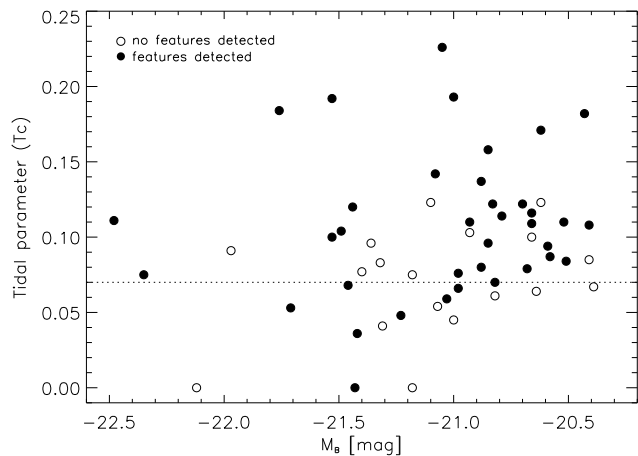


Figure 5. Corrected tidal parameter values from Tal et al. (2009) for the OBEY survey versus B-band absolute magnitudes. The dotted horizontal line at $T_c=0.07$ is the boundary between galaxies with and without signs of disturbance from Tal et al. (2009). Filled circles correspond to the galaxies visually classified as disturbed in this work, whereas open circles indicate absence of morphological features.

band absolute magnitudes (see also Table 1). First, we note that there is no clear correlation between the luminosities of the galaxies and the level of disturbance of their hosts. Second, we have identified with filled circles the galaxies in the OBEY survey for which we have found signs of interaction based on our visual classification. From Figure 5 it is clear that quantitative and visual classifications do not agree completely. There is complete agreement only for the nine galaxies with $T_c > 0.13$. In fact, for five galaxies that Tal et al. 2009 classified as clearly disturbed ($T_c > 0.09$) we do not find any sign of a past interaction. After inspecting the images of these five galaxies we conclude that it is likely that the high value of T_c is due to residuals from the masking of the foreground stars and background galaxies and/or from isophotal twisting. The opposite is also true: we find disturbed morphologies in 7 galaxies with $T_c < 0.07$, which are either faint relative to their host galaxies or diffuse features that the automatic method misses. Overall, however, the total percentages of disturbance agree well between the automatic (73%) and the visual classification (67%). This vindicates the use of visual rather than quantitative detection of disturbed morphologies in this paper.

3.1.3 Classification

Considering the morphological features detected in the OBEY and EGS galaxies (only those with secure identifications in Tables 1 and 2), the sample can be divided into the following five groups:

- (1) *Galaxy pair or group in tidal interaction.* Galaxy pairs showing bridges, or co-aligned distorted structures.
- (2) *Galaxies showing tidal features.* Galaxies showing shells, fans, tails, amorphous haloes, and irregular features.
- (3) *Multiple nuclei.* Galaxies with a companion lying inside a 10 kpc radius, according to the theoretical definition employed by Hoessel (1980) and Smith & Heckman (1989).

(4) *Dust features.* Galaxies presenting dust features as the only sign of disturbance.

(5) *Isolated galaxies with no sign of interaction.* Objects in which we cannot confidently identify morphological peculiarities.

Note that these categories are not exclusive because some galaxies show more than one of the morphological features described above (see Table 1). Initially we considered objects in groups 1, 2, 3, and 4 as showing disturbed morphologies consistent with them having been involved in a galaxy interaction/merger, whilst galaxies classified in the fifth group were classified as undisturbed. Based on this classification, in RA11 we found that 85% of the PRG sample are very likely interacting objects or the result of a past merger event. However, *dust* features by themselves may not necessarily be a sign of galaxy interactions. Note that, while small-scale dust is often taken as an observational signature for recent mergers (e.g., van Dokkum & Franx 1995), it may also be associated with cooling flows in central cluster galaxies (e.g., Fabian et al. 1994; Hansen et al. 1995; Edge et al. 1999, 2010). If we do not consider dust as a sign of morphological disturbance related to mergers and interactions, then the percentage of PRGs in the 2Jy sample presenting evidence for interactions is 78%. In Table 3 we show the percentages of interacting galaxies (those classified in groups 1, 2, or 3) for i) the PRGs sample at $z < 0.2$ and the OBEY survey, and ii) the PRGs sample at $0.2 \leq z < 0.7$ and the EGS sample.

Thus, if we only consider the galaxies classified in groups 1, 2, and 3, we find that 62% of the PRGs at $z < 0.2$ show signs of interactions. However, it is worth considering the percentage of disturbance after excluding the WLRGs (shown between parentheses in Table 3). As explained in the Introduction, it has been proposed that WLRGs are powered by hot gas accretion from their X-ray coronae, rather than by the classical AGN cold gas accretion (see also Section 5.2.2. in RA11). Thus, if we consider SLRGs only, the percentage of PRGs showing signs of interactions increases to 93%, which is higher than the 67% that we measure for the elliptical galaxies in the OBEY survey. On the other hand, 95% of the PRGs at $0.2 \leq z < 0.7$ (either including or excluding the only WLRG in this redshift range) show signs of interaction, compared with 55% in the EGS sample (57% if we consider only ellipticals and not the possible disks; column 7 in Table 2). Thus, there appears to be more evidence for galaxy interactions in the PRG sample than in the control samples at all redshifts, although the relatively small size of the PRG sample means that the difference is only significant at the $\sim 2\sigma$ level (for the comparison between the $0.2 \leq z < 0.7$ PRG and EGS samples). However, it is necessary to consider the surface brightnesses of the features in order to make a proper comparison with the control sample morphologies, since we know that, for example, the OBEY images reach much lower effective surface brightnesses than our GMOS-S images of the PRGs. This comparison provides firmer evidence for differences between the PRG and quiescent elliptical galaxy samples and it is discussed in Section 3.1.4.

In terms of the merger scenario, we appear to be observing some of the galaxies in the PRG and the two control samples *before* the final coalescence of the nuclei of the in-

interacting system. The galaxies classified in groups 1 (*galaxy pair or group in tidal interaction*) and 3 (*multiple nuclei*) would correspond to systems observed before the coalescence of the merging nuclei, whereas those in group 2 (*galaxies presenting any sign of disturbance*) would correspond to more evolved systems (coalescence or post-coalescence). The percentage of galaxies in the PRG, OBEY, and EGS samples belonging to each of these groups is shown in Table 3.

In RA11 we showed that, if PRGs are triggered as a consequence of an interaction between galaxies, it is possible for this to happen any stage of the interaction (before, during, or after the two galaxy nuclei coalesce; see also Tadhunter et al. 2011 on basis of young stellar population properties). In fact, we found that more than one-third of the PRGs in the full 2Jy sample are observed in a pre-coalescence phase (galaxies classified in either group 1 or 3). Interestingly, for both the low and intermediate redshift sub-samples, we find that the proportion of PRGs that are in the pre-coalescence phase is a factor 2–3 higher than that of the quiescent elliptical galaxies in a similar phase (see Table 3). There is also evidence for an increase in the proportion of pre-coalescence systems with redshift for both the PRG and quiescent samples (see Table 3). However, observations of larger samples will be required to put those trends on a more solid statistical footing.

The lack of dust features in the control sample as compared to the PRG sample is also interesting. For the OBEY survey we find that only 7% of the elliptical galaxies show dust, whereas for the PRGs at $z < 0.2$ the percentage increases to 25% (21% for the SLRGs). This agrees with the $\sim 30\%$ of dust features found from optical HST images of radio galaxies at $z < 0.5$ (de Koff et al. 1996, 2000). Dust can either be produced by mass loss from evolving red giant stars (Knapp et al. 1989; Athey et al. 2002), or accreted during galaxy interactions (Goudfrooij et al. 1994; van Dokkum & Franx 1995). If the dust is accreted in mergers/interactions, then we expect to find a higher incidence of dust features in the PRGs than in the quiescent ellipticals, mirroring the difference found for signs of disturbance in general between the two populations (see Table 7). On the other hand, at higher redshifts neither the galaxies in the EGS nor in the SLRG sample at $0.2 \leq z < 0.7$ show dust features. This apparent lack of dust at higher redshifts in both the radio and the quiescent galaxies is likely to be due to a resolution effect, since dust lanes, with typical scales of $\sim 1\text{--}5$ kpc, will be poorly resolved in the ground-based data employed here and in RA11 for galaxies at such redshifts.

We have classified the galaxies in the OBEY and EGS samples in the same manner as the PRGs and compared them. However, as we mentioned in Section 2.1, from the comparison between the M_B histograms of the PRGs at $z < 0.2$ and the OBEY sample shown in Figure 1, there is only a 4% chance that the two distributions are drawn from the same parent population according to the KS test. In order to confirm that this difference does not produce any bias in the statistics of morphologically disturbed systems, we have split the OBEY sample into two absolute magnitude bins using the median value of $M_B = -20.98$ mag. We find 59% of disturbance (filled circles in Figure 5) in the sub-sample with $M_B < -20.98$ mag (27 galaxies) and 75% if we consider $M_B \geq -20.98$ mag (28 galaxies). Thus, we find a slightly larger percentage of disturbed morphologies for the

lower luminosity ellipticals. The galaxies in the OBEY survey are less luminous than the PRGs on average (see Figure 1), and thus, any bias caused by this effect would result in an enhancement of the number of disturbed morphologies in the OBEY sample relative to the PRGs at $z < 0.2$. However, by looking at Figure 5 is clear that there is no correlation between M_B and the level of disturbance of the galaxies in the OBEY sample. Although for the galaxies in the EGS sample the M_B distribution is more similar to that of the PRGs at $0.2 \leq z < 0.7$ (0.18 of significance according to the KS test; see Section 2.2), we have performed the same test as for the ellipticals in the OBEY survey. By splitting the EGS sample into galaxies brighter and fainter than $M_B = -21.25$ mag (i.e. the median value), we find 60% and 50% of disturbance respectively (53 and 54 galaxies included in each bin respectively). Thus, we do not find any significant correlation between the levels of morphological disturbance and the luminosity of the elliptical galaxies in either the EGS or OBEY samples.

3.1.4 Surface brightnesses

The main result of RA11 is that 85% (78% if we do not consider galaxies with dust features only) of the 2Jy sample of PRGs show peculiar optical morphologies at relatively high levels of surface brightness: 1) $\tilde{\mu}_V = 24.0$ mag arcsec $^{-2}$ and $\Delta\mu_V = [22.1, 26.2]$ mag arcsec $^{-2}$ at $z < 0.2$; and 2) $\tilde{\mu}_V = 23.5$ mag arcsec $^{-2}$ and $\Delta\mu_V = [21.3, 25.1]$ mag arcsec $^{-2}$ at $0.2 \leq z < 0.7$.

In Tables 4 and 5 we report apparent surface brightnesses (μ_V in the case of the OBEY survey and μ_{RC} for the EGS sample) for all the secure detections of *tails, fans, shells, bridges, amorphous haloes* and *irregular features* detected in the control sample images. These surface brightnesses have been obtained exactly in the same manner as those reported in RA11. We first calculated the averaged number of counts of each feature using small apertures, and then repeated the process, using the same aperture, in several regions of the galaxy on either side of the feature to subtract the sky and the diffuse host galaxy background. In order to test the robustness of this technique, CRA and PB measured the surface brightnesses of the same features for some of the galaxies independently, obtaining differences below 0.1 mag.

For the OBEY survey, in Table 4 we report the μ_V^{corr} values, obtained after correcting μ_V from Galactic extinction Schlegel et al. (1998). For the galaxies in the EGS sample, which are at redshifts $0.2 \leq z < 0.7$, the surface brightnesses were K-corrected, using the values reported in Frei & Gunn (1994) and Fukugita et al. (1995) for elliptical galaxies, in addition to the $(1+z)^4$ cosmological dimming and extinction corrections⁷. The final μ_{RC}^{corr} values for the EGS sample are shown in Table 5. We finally transform the μ_{RC}^{corr} values into V-band measurements to compare with the OBEY sample and the PRGs by assuming colours of elliptical galaxies from Frei & Gunn (1994) and Fukugita et al. (1995).

⁷ Values of E(B-V) from Schlegel et al. (1998) were used for each of the four Suprime-Cam images in the EGS, together with the Cardelli et al. (1989) extinction law to derive the corresponding A_{RC} values.

Morphology	Group	PRG Sample $z < 0.2$	OBEY survey	PRG Sample $0.2 \leq z < 0.7$	EGS sample
Signs of interaction	1,2,3	62% (93%)	67%	95% (95%)	55% (57%)
Pre-coalescence	1,3	21% (21%)	7%	50% (50%)	20% (24%)
Coalescence or post-coalescence	2*	42% (72%)	60%	45% (45%)	35% (33%)
No signs of interaction	4,5	37% (7%)	33%	5% (5%)	45% (43%)

Table 3. Classification of all the galaxies in the PRG, OBEY and EGS samples. Sources belonging to groups 1 and 3 are considered as pre-coalescence systems, those in group 2 are likely coalescence or post-coalescence scenarios, and finally, galaxies classified in groups 4 and 5 do not show signs of interaction. * Those galaxies classified as (2,3) or (1,2) in Tables 1, 2, and Table 1 in RA11 are considered as pre-coalescence systems here, although they belong to group 2 as well. Percentages between parentheses correspond to SLRGs in the PRG sample (columns 3 and 5) and to elliptical galaxies only in the EGS sample (column 6).

We have chosen K-corrections and colour transformations for elliptical galaxies, but some of the features may be produced in mergers involving small disk galaxies and/or there can be local star formation taking place in tidal features associated with the interaction. In such cases the galaxy colours would be more similar to those of spiral galaxies. In order to assess the importance of this effect, in RA11 we re-calculated the μ_V^{corr} values of the features by using K-corrections and colours of Sbc-type spiral galaxies and confirmed that they did not change significantly ($\sim 0.1 \text{ mag arcsec}^{-2}$).

The comparison between μ_V^{corr} values measured for the features detected in our PRGs and those for the OBEY survey is shown in Figure 6(a) and Table 6. In Figure 6(b) we show the same comparison, but considering only the brightest disturbed feature of each galaxy. According to the KS test, the PRG and OBEY distributions shown in Figures 6(a) and 6(b) are different at the 99.9% significance level ($> 3\sigma$).

The median depth and range of the detected features in the OBEY galaxies are $\tilde{\mu}_V^{corr} = 25.8 \text{ mag arcsec}^{-2}$ and $\Delta\mu_V = [23.4, 28.2] \text{ mag arcsec}^{-2}$, respectively. Thus, the features detected in PRGs at $z < 0.2$ are $\sim 2 \text{ mag}$ brighter than in their quiescent counterparts. In fact, if we only consider the features in the OBEY survey which have surface brightnesses within the range of the PRGs at $z < 0.2$ (i.e. $\mu_V^{corr} \leq 26.2 \text{ mag arcsec}^{-2}$, which is exactly the same if we consider SLRGs only; see Table 6), the percentage of objects with morphological disturbance goes down to 53%. Thus, when the same range of surface brightness is considered, the proportion of interacting systems found in the PRG sample is considerably larger (93% if we consider SLRGs only) than that found for quiescent ellipticals.

In Figure 7 and Table 6 we show the same comparisons, but this time for the galaxies in the EGS sample and the $0.2 \leq z < 0.7$ PRGs. Note that for the galaxies with “multiple nuclei” as the only detected feature there are no measurements of surface brightnesses and thus, they are not included in Figures 6 and 7. However, those galaxies have been considered in the statistics presented in Table 7. The differences between the two distributions in Figure 7(a) are significant at the 2σ level: 98% significance according to the KS test and 95% if we consider the brightest features only (Figure 7(b)). We measured $\tilde{\mu}_V^{corr} = 24.2 \text{ mag arcsec}^{-2}$ and $\Delta\mu_V = [22.3, 26.3] \text{ mag arcsec}^{-2}$ for the EGS sample. We emphasise that the results obtained by including or excluding objects with possible disk components (PD) are exactly the same. Thus, for the sake of simplicity, in the following

we will consider the whole sample of 107 galaxies (including ellipticals and possible disks; see Table 1).

The surface brightnesses measured for the features of the PRGs at $0.2 \leq z < 0.7$ are $\sim 1 \text{ mag}$ brighter than those of quiescent red galaxies of similar masses and redshifts. If we only consider the galaxies in the EGS with features within the same μ_V^{corr} range as the PRGs at $0.2 \leq z < 0.7$ ($\mu_V^{corr} \leq 25.1 \text{ mag arcsec}^{-2}$), the percentage of objects with disturbed morphologies is 48%. Again, this percentage is considerably lower than the number of interacting systems found for the PRG sample at $0.2 \leq z < 0.7$ (95%; see Table 7). In these statistics we have included the systems classified as “multiple nuclei”, even if it is not possible to calculate a value of μ_V^{corr} for this type of morphology.

4 DISCUSSION

4.1 Comparison between active and quiescent elliptical galaxies

As explained in Section 1, if galaxy interactions are the main triggering mechanism for radio-loud AGN activity, then we expect to find stronger and more common signs of morphological disturbance in the radio source host galaxies than in the general population of quiescent elliptical galaxies. The majority of quiescent luminous ellipticals were likely assembled through gas-poor mergers (van Dokkum 2005), whereas to trigger and feed a powerful radio source it is likely to require a larger gas supply. According to simulations, the morphological signatures of gas-rich interactions (such as tidal tails, shells, bridges, etc.) are brighter than those produced in gas-poor interactions (Naab et al. 2006; Bell et al. 2006; McIntosh et al. 2008).

We have compared the morphologies of the 2Jy sample of radio galaxies with first, a sample of ellipticals at redshift $z < 0.2$, and second, with a sample of early-type galaxies at $0.2 \leq z < 0.7$. We find that a significant fraction of quiescent elliptical galaxies in the two control samples show evidence for disturbed morphologies at relatively high levels of surface brightness, which are likely the result of past or on-going galaxy interactions. However, the morphological features detected in the galaxy hosts of the PRGs (e.g. tidal tails, shells, bridges, etc.) are up to 2 magnitudes brighter than those present in their quiescent counterparts.

In fact, when we consider the same surface brightness limits for the features in the quiescent galaxies and in the PRGs (note that these limits are different in each redshift bin; see Table 7), we find that the proportion of disturbed

ID	Morphology	μ_V (mag arcsec ⁻²)	μ_V^{corr} (mag arcsec ⁻²)
NGC 0584	2S,B	25.6, 26.9, 25.9	25.5, 26.8, 25.8
NGC 0596	S,F	25.7, 26.1	25.6, 26.0
NGC 0720	2F	26.0, 26.0	25.9, 25.9
NGC 1199
NGC 1209	T,3F,[D]	27.7, 25.5, 25.2, 25.8	27.6, 25.4, 25.1, 25.7
NGC 1399
NGC 1395	3S	25.9, 26.4, 26.1	25.8, 26.3, 26.0
NGC 1407
NGC 2865	3S,2T,[D]	24.6, 23.7, 24.7, 25.8, 26.0	24.3, 23.4, 24.4, 25.5, 25.7
NGC 2974	S,[D]	23.9	23.7
NGC 2986	[B]
NGC 3078
NGC 3258	[2N]
NGC 3268	S	25.5	25.2
NGC 3557B	2I	25.1, 25.0	24.8, 24.7
NGC 3557	F,[S]	25.5	25.2
NGC 3585	2S	26.0, 25.4	25.8, 25.2
NGC 3640	S,4F	26.5, 26.1, 25.5, 24.9, 23.9	26.4, 26.0, 25.4, 24.8, 23.8
NGC 3706	2S	23.9, 25.3	23.6, 25.0
NGC 3904	S	25.2	25.0
NGC 3923	4S	25.8, 25.3, 24.8, 24.4	25.6, 25.1, 24.6, 24.2
NGC 3962	S	25.7	25.6
NGC 4105	2F,T	26.1, 25.7, 25.3	25.9, 25.5, 25.1
NGC 4261	T,F	26.8, 26.7	26.7, 26.6
NGC 4365	F	25.9	25.8
IC 3370	F,S,D	25.3, 25.3	25.0, 25.0
NGC 4472
NGC 4636	F	26.9	26.8
NGC 4645
NGC 4697
NGC 4696	S,D	26.3	26.0
NGC 4767	2S,[D]	23.7, 26.0	23.4, 25.7
NGC 5011
NGC 5018	3T,3S,[D]	25.1, 25.7, 27.1, 24.7, 26.1, 24.5	24.8, 25.4, 26.8, 24.4, 25.8, 24.2
NGC 5044
NGC 5061	T,S	26.0, 25.0	25.8, 24.8
NGC 5077	[S],[D]
NGC 5576	3T,S	26.7, 25.3, 25.8, 25.9	26.6, 25.2, 25.7, 25.8
NGC 5638	T,S	28.1, 28.3	28.0, 28.2
NGC 5812	T	27.8	27.5
NGC 5813
NGC 5846	3S,2N	26.7, 26.6, 27.0	26.5, 26.4, 26.8
NGC 5898	3T,D,2N	27.3, 26.5, 27.6	26.9, 26.1, 27.2
NGC 5903
IC 4797	T,I,[D]	26.4, 25.8	26.2, 25.6
IC 4889	F	26.4	26.2
NGC 6861	D
NGC 6868
NGC 6958	3S,[D]	26.2, 26.6, 28.1	26.1, 26.5, 28.0
NGC 7029
NGC 7144
NGC 7196	S,[D]	27.1	27.0
NGC 7192	S	27.5	27.4
IC 1459	4S	26.8, 26.6, 26.1, 26.5	26.7, 26.5, 26.0, 26.4
NGC 7507	S	28.1	28.0

Table 4. Surface brightness measurements of the detected features in the V-band (Vega system). Column 2 lists our morphological classification (same as in Table 1). Apparent surface brightnesses and those corrected of galactic extinction (A_V) for secure identifications of T, F, S, B, A and I are given in Columns 3 and 4, respectively. Brackets in Column 2 indicate uncertain identification.

IRAC ID	Dimming (mag arcsec ⁻²)	Type	Morphology	μ_{RC} (mag arcsec ⁻²)	μ_{RC}^{corr} (mag arcsec ⁻²)
004162	1.7	E
006612	1.2	E	B,F,[D],[T]	23.5, 24.2	21.9, 22.6
006613	1.1	E	B	24.7	23.1
056690	1.8	E	[A],[B]
060191	2.0	E	F	25.1	22.1
060958	1.5	PD	T,[A],[B]	26.2	24.2
061249	2.2	PD	[T]
066105	1.8	E	[A]
067417	1.4	E
072533	1.2	E	S	25.2	23.5
073519	1.7	E	[A]
074777	1.5	E	[S]
074924	1.5	E
077695	1.3	PD	T	26.2	24.5
079968	2.0	E	F	26.7	23.5
082325	1.9	E	[F]
083714	1.8	E	F	25.8	23.2
088031	1.8	E	F	26.8	24.3
090430	1.4	E	A,F,[B]	25.1, 26.2	23.1, 24.3
092065	1.9	E	B	25.3	22.4
092765	1.3	PD	[A],[T]
093764	1.4	E	[S]
094231	1.5	E	2F,[T]	25.0, 25.2	22.9, 23.1
094966	1.6	E	2T	26.0, 26.4	23.7, 24.1
095727	1.4	E	F,S	27.2, 25.7	25.3, 23.7
099954	1.0	E	[T]
102757	0.9	E	2S	26.1, 26.2	25.0, 25.0
102982	2.0	E	F	25.0	21.8
103198	1.4	E	2N,F,S	26.5, 25.4	24.6, 23.5
104038	1.6	E	B	24.4	22.0
104729	2.1	PD	A	25.5	22.1
105193	0.9	E	[S]
106324	1.0	E	[T]
106984	1.6	PD	A,[I]	26.2	23.9
111427	1.2	E	2N,T,2I	24.5, 26.4, 25.7	22.9, 24.8, 24.1
112580	1.8	E	[B]
113088	1.7	E	[B]
113577	2.2	PD	[A]
114966	2.1	PD	2T,S	25.2, 25.3, 26.2	21.9, 22.1, 22.9
115327	1.3	E	2F,[T]	27.3, 27.6	25.6, 25.8
115594	1.2	E	2N,T	26.5	24.9
118942	1.4	E
119696	1.8	E	B,F	24.9, 26.2	22.3, 23.6
122098	0.9	PD
124509	1.3	PD	B,2T,F	24.3, 24.1, 27.3, 27.0	22.6, 22.4, 25.6, 25.3
125663	1.8	E	[F]
126918	1.7	E	F,[B]	25.8	23.2
127241	2.0	PD
127457	1.7	E	2N,A	24.8	22.2
128074	1.3	E	B,[F]	26.9	25.2
128416	2.0	PD
132682	1.2	E
135859	1.4	E	[I]

morphologies in the quiescent population is considerably smaller (53% at $z < 0.2$ and 48% at $0.2 \leq z < 0.7$) than for the PRGs (93% at $z < 0.2$ and 95% at $0.2 \leq z < 0.7$, considering SLRGs only). This indicates that galaxy interactions are likely to play a role in the triggering of PRG activity.

However, it is important to recognise that a proportion of the quiescent elliptical galaxy population *do* show disturbed features at a similar level of surface brightness to the

PRGs. Moreover, even if the proportion of such objects is relatively small, their volume density could be considerably larger than that of the (rare) PRGs. This raises the question of how the populations of disturbed elliptical galaxies and PRGs are related. The simplest assumption we can make is that *all* morphologically disturbed elliptical galaxies go through a radio-loud AGN phase at some stage in the galaxy interaction that causes the disturbed features. In this case,

IRAC ID	Dimming (mag arcsec ⁻²)	Type	Morphology	μ_{R_C} (mag arcsec ⁻²)	$\mu_{R_C}^{corr}$ (mag arcsec ⁻²)
138794	1.8	E	[T]
139190	1.6	E
140456	1.1	PD	2T	24.5, 25.3	23.0, 23.8
140758	1.6	E	S	26.0	23.8
141714	1.6	PD	[B],[S]
143149	1.4	E	T	25.8	23.9
143536	1.8	PD	[T]
145098	1.2	E	A,T	25.7, 27.2	24.0, 25.6
145434	1.7	PD	4T	24.6, 25.7, 25.1, 25.7	22.2, 23.2, 22.6, 23.2
146298	2.0	E	[A]
152722	1.7	PD	[F]
156161	1.1	E	T	24.5	23.0
157751	1.7	E
157878	1.6	E	F	26.3	24.0
159123	1.9	PD	T	25.7	22.8
159936	1.5	E	2N
160442	1.7	E	B,A	26.5, 25.6	24.1, 23.2
160500	1.3	PD	B,2T	26.7, 26.0, 25.4	24.9, 24.3, 23.7
161724	1.3	PD	[F]
165265	2.2	E	B,T	25.7, 26.2	22.0, 22.4
166730	1.3	E	S,T	25.8, 27.0	23.9, 25.1
169386	1.7	PD
172474	1.8	E	T,B,F	26.3, 27.9, 26.6	23.7, 25.3, 23.9
173901	1.2	E
175347	2.0	E	S,[B]	26.4	23.2
175590	1.9	E	[A]
177990	1.0	PD	F,[2N]	26.1	24.8
178118	1.6	E
178724	1.8	E	A	26.6	23.9
178868	1.4	PD	F	26.1	24.2
180420	1.9	E	2N,2T,[B]	25.8, 26.2	22.9, 23.4
181402	1.4	E	[I],[A]
181444	1.2	E	2S,[I]	25.5, 24.8	23.9, 23.3
181736	1.7	PD
181914	1.3	PD
182762	1.5	PD	[F]
183081	1.3	E	F,[T]	26.8	24.9
183836	1.6	E	[S]
184041	1.8	E	F,S	25.4, 26.5	22.6, 23.7
184315	1.8	PD	2N
186058	1.9	PD	[A]
189727	2.1	PD
190795	1.8	PD	T,S	25.2, 26.1	22.6, 23.4
193464	1.5	E	2N,F	25.5	23.4
193507	1.7	E	2N,[B]
193737	1.7	E
193974	1.5	E	[S]
194092	1.8	E	[T]
196827	1.4	E	T	26.6	24.7
198295	1.9	E	[S]
199503	1.7	PD	T	26.8	24.3
202111	1.0	E	[S]
204161	2.1	E	A,[B]	26.0	22.6
204944	1.1	PD	T,S	26.3	24.9

Table 5. Surface brightness measurements of the detected features in the R_c-band (AB system). Column 2 corresponds to the surface brightness dimming from NED, column 3 indicates whether a galaxy has been visually classified as an elliptical (E) or as a possible disk (PD), and column 4 lists our morphological classification as in Table 1. Apparent and corrected (including galactic extinction, dimming, and k-corrections) surface brightness for secure identifications of T, F, S, B, A and I are given in Columns 5 and 6, respectively. Brackets in column 4 indicate uncertain identification.

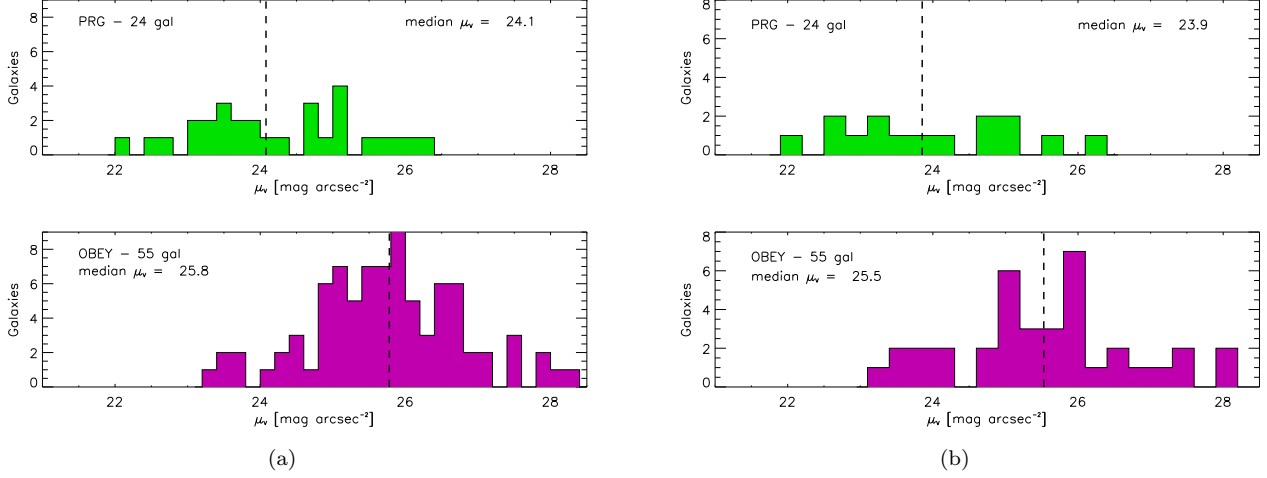


Figure 6. (a) Comparison between the μ_V^{corr} of the 24 PRGs in the 2Jy sample at $z < 0.2$ (top panel) and those of the elliptical galaxies in the OBEY survey (bottom panel). (b) Same as in (a) but considering the brightest feature in each source only.

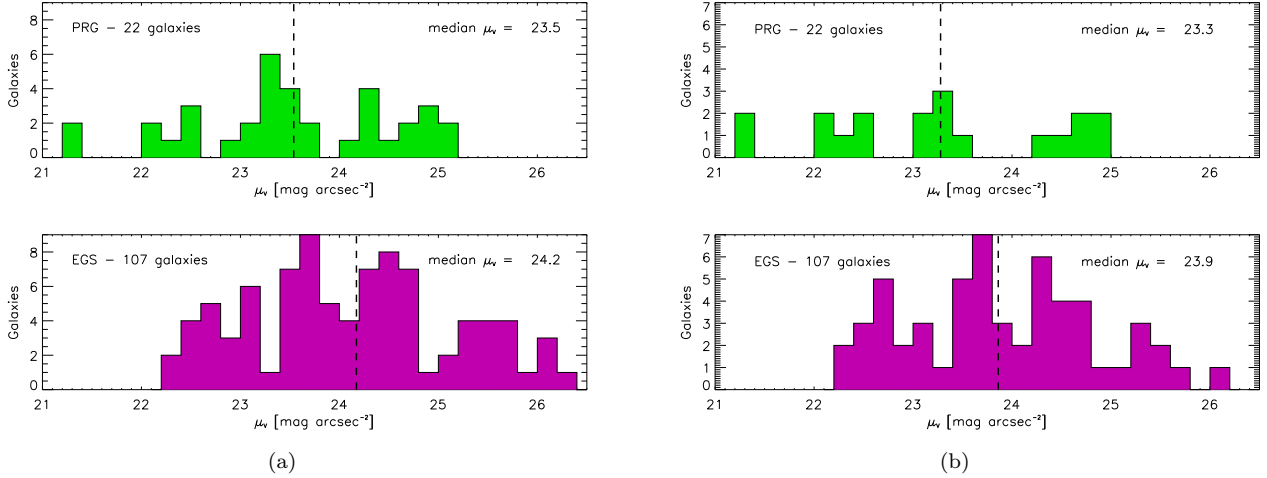


Figure 7. (a) Comparison between the μ_V^{corr} of the 22 PRGs in the 2Jy sample at $0.2 \leq z < 0.7$ (top panel) and those of the red galaxies in the EGS sample (bottom panel). (b) Same as in (a) but considering the brightest feature in each source only.

the total volume density of PRGs (ρ_{PRG}) is related to the total volume density of disturbed elliptical galaxies (ρ_{DE}) by the following equation:

$$\frac{\rho_{PRG}}{\rho_{DE}} = 0.01 \left(\frac{t_{PRG}}{10 \text{ Myr}} \right) \left(\frac{t_{DF}}{1 \text{ Gyr}} \right)^{-1}, \quad (1)$$

where t_{PRG} is the duty cycle of the powerful radio-loud AGN activity and t_T the timescale over which the tidal features associated with a particular galaxy interaction remain visible above the surface brightness limit of the observations. Typically, PRGs are expected to remain active over a period of $t_{PRG} \sim 10 - 100$ Myr (Leahy et al. 1989; Blundell et al. 1999; Shabala et al. 2008), while the tidal features will remain visible on a timescale of ~ 1 Gyr (Le Fèvre et al. 2000; Patton et al. 2002; Conselice et al. 2003; Kawata et al. 2006). Therefore we should expect the PRG to make up a fraction $\rho_{PRG}/\rho_{DE} \sim 0.01 - 0.1$ of the full population of disturbed elliptical galaxies assuming that all such galaxies go through a radio-loud phase.

A direct estimate of the volume density of PRGs can be obtained by integrating the radio luminosity function of Willott et al. (2001) above the lower radio power limit of the $0.05 < z < 0.7$ 2Jy sample ($P_{151}^{lim} \text{ MHz} \approx 1.3 \times 10^{25} \text{ W Hz}^{-1} \text{ sr}^{-1}$). We find $\rho_{PRG} = 2 \times 10^{-7} \text{ Mpc}^{-3}$ for $z=0$ and $\rho_{PRG} = 1 \times 10^{-6} \text{ Mpc}^{-3}$ for $z=0.5$ (corrected to our assumed cosmology). Similarly, an estimate of the volume density of disturbed elliptical galaxies can be made by integrating the optical luminosity function for red sequence galaxies above the lower B-band luminosity limit of the PRG and control samples ($M_B = -20.3$ mag), then multiplying by the fraction of ellipticals with disturbed features of similar surface brightness to the PRG ($f_D \sim 0.5$). For low redshifts we integrate the luminosity function for red sequence galaxies from Baldry et al. (2004), obtaining $\rho_{DE} = 2 \times 10^{-4} \text{ Mpc}^{-3}$, while for higher redshifts we integrate the $z = 0.5$ luminosity function of Faber et al. (2007), obtaining $\rho_{DE} = 4 \times 10^{-4} \text{ Mpc}^{-3}$. By comparing the volume densities of PRGs and disturbed ellipticals estimated in this way we find: $\rho_{PRG}/\rho_{DE} \sim 10^{-3}$

Morphology	PRG Sample $z < 0.2$		OBEY survey		PRG Sample $0.2 \leq z < 0.7$		EGS sample	
	$\tilde{\mu}_V^{corr}$	$\Delta\mu_V$	$\tilde{\mu}_V^{corr}$	$\Delta\mu_V$	$\tilde{\mu}_V^{corr}$	$\Delta\mu_V$	$\tilde{\mu}_V^{corr}$	$\Delta\mu_V$
All features	24.1 (24.3)	22.1 - 26.2 (22.6 - 26.2)	25.8 ...	23.4 - 28.2 ...	23.5 (23.5)	21.3 - 25.1 (21.3 - 25.1)	24.2 ...	22.3 - 26.3 ...
Brightest features	23.8 (24.1)	22.1 - 26.2 (22.6 - 26.2)	25.5 ...	23.4 - 28.0 ...	23.3 (23.3)	21.3 - 24.9 (21.3 - 24.9)	23.9 ...	22.3 - 26.1 ...

Table 6. Median values and ranges of the surface brightness measurements of the PRG, OBEY, and EGS samples. Values considering all the features detected (two top rows) and the brightest feature of each galaxy (bottom rows) are listed. Surface brightnesses between parentheses correspond to SLRGs in the PRG sample.

Morphology	Group	PRGs $z < 0.2$	OBEY	PRGs $0.2 \leq z < 0.7$	EGS
Signs of interaction	1,2,3	62% (93%)	53%	95% (95%)	48% (52%)

Table 7. Percentages of disturbance found for the PRGs at $z < 0.2$ and the OBEY survey at the same level surface brightness level ($\mu_V^{corr} \leq 26.2 \text{ mag arcsec}^{-2}$) and the same for the PRGs at $0.2 \leq z < 0.7$ and the EGS survey ($\mu_V^{corr} \leq 25.1 \text{ mag arcsec}^{-2}$). In these numbers we include galaxies classified as multiple nuclei systems (group 3). Percentages between parentheses correspond to SLRGs in the PRG sample (columns 3 and 5) and to elliptical galaxies only in the EGS sample (column 6).

for $z < 0.2$ and $\rho_{PRG}/\rho_{DE} \sim 2 \times 10^{-3}$ for $z = 0.5$. These proportions are considerably lower – by a factor of five or more – than those obtained above, based on the PRG duty cycle and the assumption that all disturbed elliptical galaxies go through a radio-loud phase ($\rho_{PRG}/\rho_{DE} \sim 0.01 - 0.1$). We conclude that only a small proportion ($\lesssim 20\%$) of interacting giant elliptical galaxies with absolute magnitudes $M_B < -20.3 \text{ mag}$ are capable of hosting powerful radio sources with radio powers $P_{151 \text{ MHz}}^{lim} > 1.3 \times 10^{25} \text{ W Hz}^{-1} \text{ sr}^{-1}$ for the requisite timescales.

Clearly, while undergoing a galaxy interaction of *some type* may be necessary to trigger powerful radio jets in a giant elliptical galaxy, it is not by itself sufficient. Other potentially important factors include: the degree of gas richness of the interacting galaxies, their mass ratio, the orbital parameters of the interaction, the masses of the galaxy bulges and associated supermassive BHs, and the BHs spin. For example, our classification of morphological disturbance in elliptical galaxies is relatively crude and does not precisely distinguish the type of galaxy interaction (e.g. whether “wet” or “dry”, minor or major). Therefore it is possible that only a minority of the disturbed elliptical galaxies in our control samples are undergoing the *precise type* of interaction that leads to the triggering of powerful radio-loud AGN activity.

Finally, we note that there is an important caveat to bear in mind when making the comparison between the PRG and control samples. We have matched the comparison samples in galaxy luminosity, redshift, and depth of observations (see Section 3.1.4 on the latter), but we have not considered the environments of the galaxies. The environment may affect the comparison in two ways. First, if a specific type of galaxy interaction is required to trigger a PRG (e.g. a major, gas-rich merger), then that type of interaction may be favoured by a particular environment (e.g. group rather than cluster; see Hopkins et al. 2008b). Second, the tidal effects associated with high density environments can rapidly disrupt the morphological structures (e.g. shells or ripples; Malin & Carter 1983) that we use to classify the galaxies in our samples. Indeed, Tal et al. (2009) and Malin & Carter (1983) explored the relationship between galaxy morphology

and environment in their samples of nearby elliptical galaxies and found that the ellipticals in clusters generally appear less disturbed than those in group and field environments.

Despite the lack of quantification of the galaxy environments in this paper, previous studies of radio galaxies in the local Universe have shown that, while FRI sources (generally WLRGs) favour clusters, FRII galaxies (generally SLRGs) are found in a wide range of environments, ranging from field/group to moderately rich clusters (Prestage & Peacock 1988; Smith & Heckman 1990; Zirbel 1997), although there is some evidence that the environments of FRII objects become richer with redshift (e.g. Hill & Lilly 1991). As noted in Section 2.1, the low redshift OBEY control sample covers a mix of environments that is similar to that of the FRIIs in the local Universe, but less rich on average than that of local FRI galaxies. However, our conclusions based on the comparison with the control samples would only likely be affected by environmental issues if the control samples were *more* biased towards rich environments than our PRG sample. At present we have no evidence that this is the case, but the whole issue of matching control sample environments and the dependence of the degree of morphological disturbance on environment clearly warrants further investigation.

4.2 Evolution of elliptical galaxies from $z \sim 0.7$

By comparing the galaxies in the OBEY and EGS samples, we can study how the morphologies of elliptical galaxies evolve from redshift $z=0.7$ and compare with the predictions of galaxy evolution models. Elliptical galaxies are key to investigate the history of galaxy mass assembly, since they dominate the high-end of the local luminosity function. While many studies support a scenario in which old (1-4 Gyr) and massive ($M_* > 10^{11} M_\odot$) ellipticals passively evolve from redshift $z \sim 1$ (e.g. Bundy et al. 2006 and references therein), others argue for a major role of dry-mergers in the build-up of the most massive early-type galaxy population from $z \sim 1$ (e.g. Bell et al. 2004; Faber et al. 2007; Kaviraj et al. 2007; López-Sanjuan et al. 2011).

In Table 8 we show the percentage of disturbance found

Work	Objects	Sample	Redshift	$\Delta\mu_V$ considered (mag arcsec $^{-2}$)	Signs of interaction
Malin & Carter (1983)	QE	137	<0.01	$\lesssim 25.5$	$\sim 10\%$
OBEY survey	QE	55	<0.01	[23.3, 25.5]	34%
2Jy sample	SLRGs	14	0.05-0.2	[22.1, 25.5]	79%
EGS sample	ET	107	0.2-0.7	[22.3, 25.5]	53% (57%)
2Jy sample	SLRGs	21	0.2-0.7	[21.3, 25.1*]	95%

Table 8. Results for the OBEY, EGS and PRG samples considering features with $\mu_V \leq 25.5$ mag arcsec $^{-2}$, to compare with those found by Malin & Carter (1983) for a sample of 137 quiescent elliptical galaxies (QE) at $z < 0.01$. * For the PRGs at $0.2 \leq z < 0.7$ the dimmest feature detected has a $\mu_V = 25.1$ mag arcsec $^{-2}$. In these percentages we include galaxies with double nuclei as the only detected feature (group 3).

for the OBEY survey (elliptical galaxies in the local universe) and the EGS sample (early-type galaxies with $0.2 < z < 0.7$) only considering features brighter than $\mu_V = 25.5$ mag arcsec $^{-2}$. This value was chosen to match the limiting surface brightness of the features found by Malin & Carter (1983) for a sample of 137 elliptical galaxies at $z < 0.01$. The latter authors used visual inspection of photographic plates to search for shells and ripples, finding that only 10% of the ellipticals showed these features. This percentage is considerably lower than the 34% that we find for the OBEY survey when the same depth is considered, likely due to the limitations associated to the use of photographic images. In addition, in Malin & Carter (1983) the authors were looking for sharp, shell-like features with the galaxy at the centre of curvature, rather than more asymmetric features such as fans, tails, bridges, etc (D. Carter, private communication).

The range of absolute magnitude that we are considering by putting together the galaxies in both the OBEY and EGS samples is $M_B = [-22.5, -20.4]$ mag (see Section 2). The percentage of disturbed morphologies in the local universe is 34% and increases to 53% at $z = [0.2, 0.7]$ when the same depth is considered ($\mu_V \lesssim 25.5$ mag arcsec $^{-2}$). Thus, we find that a significant fraction of quiescent elliptical galaxies at low and intermediate redshifts show signatures of past interactions at relatively high levels of surface brightness, and that this fraction increases slightly with redshift. This is consistent with the idea that elliptical galaxies have undergone some evolution since $z = 0.7$. However, the interactions that lead to this evolution cannot, in most cases, have noticeably modified their star formation histories and masses (López-Sanjuan et al. 2011). This would explain why in the past the most massive elliptical galaxies were thought to passively evolve from $z = 1$ to $z = 0$.

5 CONCLUSIONS

We present the results from a comparison between the optical morphologies of a complete sample of 46 southern 2Jy radio galaxies at intermediate redshifts ($0.05 < z < 0.7$) and those of quiescent early-type galaxies within the same mass and redshift ranges. Based on these results, we discuss the role of galaxy interactions in the triggering of PRGs. Our major results are as follows:

- We find that a significant fraction of quiescent early-type galaxies across the full redshift range of our study show evidence for disturbed morphologies at relatively high levels

of surface brightness, which are likely the result of past or on-going galaxy interactions.

- The morphological features detected in the galaxy hosts of the 2Jy sample of PRGs (e.g. tidal tails, shells, bridges, etc.) are up to 2 magnitudes brighter than those present in their quiescent counterparts.

- The fraction of disturbed morphologies in the quiescent population is considerably smaller (53% at $z < 0.2$ and 48% at $0.2 \leq z < 0.7$) than for PRGs (93% at $z < 0.2$ and 95% at $0.2 \leq z < 0.7$, considering SLRGs only) when the same surface brightness limits are considered.

- These results support a scenario in which PRGs, which are likely triggered by interactions, represent a fleeting active phase of a subset of elliptical galaxies that have recently undergone mergers/interactions.

ACKNOWLEDGMENTS

CRA acknowledges financial support from STFC PDRA (ST/G001758/1). CRA, PGPG, and GB acknowledge the Spanish Ministry of Science and Innovation (MICINN) through project Consolider-Ingenio 2010 Program grant CSD2006-00070: First Science with the GTC (<http://www.iac.es/consolider-ingenio-gtc/>). PGPG and GB acknowledge support from the Spanish Programa Nacional de Astronomía y Astrofísica under grants AYA2009-10368 and AYA2009-07723-E. KJI is supported through the Emmy Noether programme of the German Science Foundation (DFG). This work has made use of the Rainbow Cosmological Surveys Database, which is operated by the Universidad Complutense de Madrid (UCM). This work is based in part on data collected at Subaru Telescope, which is operated by the National Astronomical Observatory of Japan. This research has made use of the NASA/IPAC Extragalactic Database (NED) which is operated by the Jet Propulsion Laboratory, California Institute of Technology, under contract with the National Aeronautics and Space Administration. The authors specially acknowledge Tomer Tal for providing access to the OBEY images, as well as David Carter, Richard Pogge, Philip Massey, Giovanni Carraro, and Carlos López-SanJuan for their valuable help. We finally acknowledge useful comments from the anonymous referee.

REFERENCES

- Allen, S. W., Dunn, R. J. H., Fabian, A. C., Taylor, G. B., Reynolds, C. S. 2006, *MNRAS*, 372, 21
- Athey, A., Bregman, J. N., Bergman, J. D., Temi, P., Sauvage, M. 2002, *ApJ*, 571, 272
- Baldry, I. K., Glazebrook, K., Brinkmann, J., Ivezić, Ž., Lupton, R. H., Nichol, R. C., Szalay, A. S. 2004, *ApJ*, 600, 681
- Balmaverde, B., Baldi, R. D., Capetti, A. 2008, *A&A*, 486, 119
- Barro, G., et al. 2011, *ApJS*, 193, 13
- Barro, G., et al. 2009, *A&A*, 494, 63
- Bell, E. F., Naab, T., McIntosh, D. H., et al. 2006, *ApJ*, 640, 241
- Bell, E. F., et al. 2004, *ApJ*, 608, 752
- Bennert, N., Canalizo, G., Jungwiert, B., Stockton, A., Schweizer, F., Peng, C. Y., Lacy, M. 2008, *ApJ*, 677, 846
- Best, P. N., Kaiser, C. R., Heckman, T. M., Kauffmann, G. 2006, *MNRAS*, 368, L67
- Blanton, M. R. 2006, *ApJ*, 648, 268
- Blundell, K. M., Rawlings, S., Willott, C. J. 1999, *AJ*, 117, 677
- Borne, K. D. 1984, *ApJ*, 287, 503
- Bundy, K., et al. 2010, *ApJ*, 719, 1969
- Bundy, K., et al. 2006, *ApJ*, 651, 120
- Buttiglione, S., Capetti, A., Celotti, A., Axon, D. J., Chibera, M. Macchetto, F. D., Sparks, W. B. 2010, *A&A*, 509, 6
- Canalizo, G., Stockton, A. 2000, *ApJ*, 528, 201
- Canalizo, G., Bennert, N., Jungwiert, B., Stockton, A., Schweizer, F., Lacy, M., Peng, C. 2007, *ApJ*, 669, 801
- Canalizo, G., Stockton, A. 2001, *ApJ*, 555, 719
- Cardelli, J.A., Clayton, G.C., Mathis, J. 1989, *ApJ*, 345, 245
- Cattaneo, A., Combes, F., Colombi, S., Bertin, E., Melchior, A.-L. 2005, *MNRAS*, 359, 1237
- Cimatti, A., Daddi, E., Renzini, A. 2006, *A&A*, 453, L29
- Cisternas, M., et al. 2011, *ApJ*, 726, 57
- Conselice, C. J., Bershady, M. A., Dickinson, M., Papovich, C. 2003, *AJ*, 126, 1183
- Cox, T. J., Jonsson, P., Somerville, R. S., Primack, J. R., Dekel, A. 2008, *MNRAS*, 384, 386
- Cox, T. J., Jonsson, P., Primack, J. R., Somerville, R. S. 2006, *MNRAS*, 373, 1013
- Croton, D. J., et al. 2006, *MNRAS*, 365, 11
- Davis, M., et al. 2007, *ApJ*, 660, 1
- de Koff, S. 2000, *ApJs*, 129, 33
- de Koff, S. 1996, *ApJs*, 107, 621
- de Vaucouleurs, G., de Vaucouleurs, A., Corwin, H. G., Jr., Buta, R. J., Paturel, G., Fouque, P. 1991, *Third Reference Catalogue of Bright Galaxies* (Springer: Berlin)
- Dicken, D., Tadhunter, C., Axon, D., Morganti, R., Inskip, K. J., Holt, J., González Delgado, R., Groves, B. 2009, *ApJ*, 694, 268
- di Matteo, P., Combes, F., Melchior, A.-L., Semelin, B. 2007, *A&A*, 468, 61
- Di Matteo, T., Springel, V., Hernquist, L. 2005, *Nature*, 433, 604
- Dunlop, J. S., McLure, R. J., Kukulka, M. J., Baum, S. A., O’Dea, C. P., Hughes, D. H. 2003, *MNRAS*, 340, 1095
- Dunlop, J. S., Peacock, J. A. 1990, *MNRAS*, 247, 19
- Edge, A. C., Oonk, J. B. R., Mittal, R., et al. 2010, *A&A*, 518, L47
- Edge, A. C., Ivison, R. J., Smail, Ian, Blain, A. W., Kneib, J.-P. 1999, *MNRAS*, 306, 599
- Ellison, S. L., Patton, D. R., Trevor Mendel, J., Scudder, J. M. 2011, *MNRAS*, in press
- Faber, S. M., et al. 2007, *ApJ*, 665, 265
- Fabian, A. C., Johnstone, R. M., Daines, S. J. 1994, *MNRAS*, 271, 737
- Feldmann, R., Mayer, L., Carollo, C. M. 2008, *ApJ*, 684, 1062
- Ferrarese, L., Merritt, D. 2000, *ApJ*, 539, L9
- Frei, Z., Gunn, J. E. 1994, *AJ*, 108, 1476
- Fukugita, M., Shimasaku, K., Ichikawa, T. 1995, *PASP*, 107, 945
- Gabor, J. M., et al. 2009, *ApJ*, 691, 705
- Gebhardt, K., Bender, R., Bower, G., et al. 2000, *ApJ*, 539, L13
- Georgakakis, A., et al. 2009, *MNRAS*, 397, 623
- Goudfrooij, P., Hansen, L., Jørgensen, H. E., Nørgaard-Nielsen, H. U. 1994, *A&AS*, 105, 341
- Greene, J. E., Ho, L. C. 2006, *ApJ*, 641, L21
- Grogin, N. A., et al. 2005, *ApJ*, 627, L97
- Groth, E. J., et al. 1994, *BAAS*, 26, 1403
- Hansen, L., Jørgensen, H. E., Nørgaard-Nielsen, H. U. 1995, *A&AS*, 297, 13
- Hardcastle, M. J., Evans, D. A., Croston, J. H. 2007, *MNRAS*, 376, 1849
- Heckman, T. M., Kauffmann, G., Brinchmann, J., Charlot, S., Tremonti, C., White, S. D. M. 2004, *ApJ*, 613, 109
- Heckman, T. M., Smith, E. P., Baum, S. A., van Breugel, W. J. M., Miley, G. K., Illingworth, G. D., Bothun, G. D., Balick, B. 1986, *ApJ*, 311, 526
- Hernquist, L., Spitzer, D. L. 1992, *ApJ*, 399, L117
- Hill, G. J., Lilly, S. J. 1991, *ApJ*, 367, 1
- Hoessel, J. G. 1980, *ApJ*, 241, 493
- Hook I., Jørgensen I., Allington-Smith J. R., Davies R. L., Metcalfe N., Murowinski R. G., Crampton D. 2004, *PASP*, 116, 425
- Hopkins, P. F., Cox, T. J., Kereš, D., Hernquist, L. 2008a, *ApJs*, 175, 390
- Hopkins, P. F., Hernquist, L., Cox, T. J., Kereš, D. 2008b, *ApJs*, 175, 356
- Hutchings, J. B. 1987, *ApJ*, 320, 122
- Kauffmann, G., Haehnelt, M. 2000, *MNRAS*, 311, 576
- Kaviraj, S., Tan, K.-M., Ellis, R. S., Silk, J. 2011, *MNRAS*, 411, 2148
- Kaviraj, S., et al. 2007, *ApJS*, 173, 619
- Kawata, D., Mulchaey, J. S., Gibson, B. K., Sánchez-Blázquez, P. 2006, *ApJ*, 648, 969
- Keel, W. C. 1996, *AJ*, 111, 696
- Knaap, G. R., Guhathakurta, P., Kim, D.-W., Jura, M. 1989, *ApJS*, 70, 329
- Koss, M., Mushotzky, R. Veilleux, S., Winter, L. 2010, *ApJ*, 716, L125
- Kormendy, J., Bender, R., Cornell, M. E. 2011, *Nature*, 469, 374
- Kormendy, J., Richstone, D. 1995, *ARA&A*, 33, 581
- Kuo, C.-Y., Lim, J., Tang, Y.-W., Ho, P. T. P. 2008, *ApJ*, 679, 1047
- Leahy, J. P., Muxlow, T. W. B., Stephens, P. W. 1989, *MNRAS*, 239, 401

- Le Fèvre, O., Abraham, R., Lilly, S. J., et al. 2000, MNRAS, 311, 565
- López-Sanjuan, C., et al. 2011, A&A, 530, 20
- Lotz, J. M., Jonsson, P., Cox, T. J., Primack, J. R. 2008, MNRAS, 391, 1137
- Magorrian, J., et al. 1998, AJ, 115, 2285
- Malin, D. F., Carter, D. 1983, ApJ, 274, 534
- Malkan, M. A., Gorjian, V., Tam, R. 1998, ApJ, 117, 25
- McIntosh, D. H., Guo, Y., Hertzberg, J., Katz, N., Mo, H. J., van den Bosch, F. C., Yang, X. 2008, MNRAS, 388, 1537
- Michard, R. 2005, A&A, 441, 451
- Miyazaki, S., et al. 2002, PASJ, 54, 833
- Naab, T., Khochfar, S., Burkert, A. 2006, ApJ, 636, L81
- Park, S. Q., et al. 2008, ApJ, 678, 744
- Patton, D. R., Pritchett, C. J., Carlberg, R. G., et al. 2002, ApJ, 565, 208
- Pérez-González, P. G., Trujillo, I., Barro, G., Gallego, J., Zamorano, J., Conselice, C. J. 2008, ApJ, 687, 50
- Prestage, R. M., Peacock, J. A. 1988, MNRAS, 230, 131
- Prugniel, P. & Heraudeau, P. 1998, VizieR Online Data Catalog, 7206, 0
- Quinn, P. J. 1984, ApJ, 279, 596
- Ramos Almeida, C., Tadhunter, C. N., Inskip, K. J., Morganti, R., Holt, J., Dicken, D. 2011, MNRAS, 410, 1550
- Schlegel, D. J., Finkbeiner, D. P., & Davis, M. 1998, ApJ, 500, 525
- Shabala, S. S., Ash, S., Alexander, P., Riley, J. M. 2008, MNRAS, 388, 625
- Smith, E. P., Heckman, T. M. 1990, ApJ, 348, 38
- Smith, E. P., Heckman, T. M. 1989, ApJ, 341, 658
- Somerville, R. S., Hopkins, P. F., Cox, T. J., Robertson, B. E., Hernquist, L. 2008, MNRAS, 391, 481
- Springel, V., Di Matteo, T., Hernquist, L. 2005, MNRAS, 361, 776
- Tadhunter, C., et al. MNRAS, 412, 960
- Tadhunter, C. N., Morganti, R., Robinson, A., Dickson, R., Villar-Martín, M., Fosbury, R. A. E. 1998, MNRAS, 298, 1035
- Tadhunter, C. N., Morganti, R., di Serego-Alighieri, S., Fosbury, R. A. E., Danziger, I. J. 1993, MNRAS, 263, 999
- Tal, T., van Dokkum, P. G., Nelan, J., Bezanson, R. 2009, AJ, 138, 1417
- Tully, R. B. 1988, Nearby Galaxies Catalog (Cambridge: Cambridge Univ. Press), 221
- van Dokkum, P. G. 2005, ApJ, 130, 2647
- van Dokkum, P. G., Franx, M. 1995, AJ, 110, 2027
- Wall, J. V., Peacock, J. A. 1985, MNRAS, 216, 179
- Wild, V., Heckman, T., Charlot, S. 2010, MNRAS, 405, 933
- Willott, C. J., Rawlings, S., Blundell, K. M., Lacy, M., Eales, S. A. 2001, MNRAS, 322, 536
- Yamada, T., et al. 2005, ApJ, 634, 861
- Zhao, Y.-H., Huang, J.-S., Ashby, M., Fazio, G., Miyazaki, S. 2009, Res. Astron. Astrophys., 9, 1061
- Zirbel, E. L. 1997, ApJ, 476, 489
- Zucca, E., et al. 2006, A&A, 455, 879